TAMPERE UNIVERSITY OF TECHNOLOGY

International Degree Programme in Radio Frequency Electronics

RANA AZHAR SHAHEEN

STABILITY ANALYSIS OF A CURRENT-SOURCED CONVERTER WHEN AN EMI FILTER IS ADDED AT THE INPUT FOR PV APPLICATIONS

Master of Science Thesis

Examiner: Professor Teuvo Suntio
Examiner and topic approved in the Faculty Council meeting on 02 February 2011

ABSTRACT

TAMPERE UNIVERSITY OF TECHNOLOGY
International Master's Degree Programme in Radio Frequency Electronics
RANA AZHAR SHAHEEN: Stability Analysis of a current-sourced converter when an EMI filter is added at the input for PV Applications
Master of Science Thesis, 73 pages, 7 Appendix pages
June 2011
Major: Radio Frequency Electronics
Minor: Switched-mode Converters
Examiner: Professor Teuvo Suntio
Keywords: Current-sourced converter, EMI filter, State-space averaging, stability

The aim of green energy is to reduce the environmental pollution as well as electromagnetic pollution generated by electronic products. The involvement of power electronics devices in photovoltaic systems brought the aspect of electromagnetic interference which could decrease the efficiency of solar panels. The generated EMI may be radiated to atmosphere or either conducted through the electronic circuitry paths which may harm the performance of other interconnected system. EMI filters are commonly used to reduce the conducted noise emission from the electronic product. In addition, to achieve the immunity from electromagnetic interference, the EMI filters should also be considered in such a way that the stability of the whole system is achieved after insertion of an EMI filter.

There is enough literature available for the implementation of EMI filter at AC side of photovoltaic power plant but not enough work has been done for EMI filters at DC side of PV power plants. This work proposes the approach of installing EMI filters at DC side of current-sourced converters for PV interfacing in solar power plants in such a way that the stability of the whole system should not be affected.

Solar cell is naturally considered as a current source, and a current-sourced converter is needed for efficient usage of output current of solar panels including an input EMI filter which should also be a current-sourced to reduce the noise voltage coming from the converter. Control loop is implemented from the input voltage in current-sourced converters so the stability has been assessed at two different points of control loop implementation from the input voltage.

Work in this thesis relies on the dynamical analysis of converter and EMI filter which is carried out by using state-space averaging technique. Different open and closed loop transfer functions are analysed at different operating points of solar panel. The main difficulty in the work was the lack of information regarding EMC standards for DC side EMI filters.

PREFACE

This Master of Science Thesis has been done at Tampere University of Technology, Department of Electrical Energy Engineering. Stability of a current-sourced converter when an input EMI filter is added for PV applications, has been analysed in this thesis. The instructor and examinre of the thesis was Professor Teuvo Suntio.

I would like to thank Professor Teuvo Suntio for giving me an opportunity to explore the world of Power Electronics in renewable energy field. Due to his continuous guidance and support I am able to understand the concepts in dynamical modelling of switching converters. I also want to thank M.Sc. Jari Leppaäho for his continuous help and support in finalizing my work. Great thanks also to all my friends, relatives and especially to my beloved mother and Mr. & Mrs. Tariq for their prayers and encouraging me during my studies.

Tampere, September 20, 2011

Rana Azhar Shaheen
Insinöörinkatu 60 D, 372
33720 Tampere

TABLE OF CONTENTS

SYMBOLS AND ABBREVIATIONS

SYMBOLS

A	Coefficient matrix
B	Coefficient matrix
C	Coefficient matrix
C	Capacitor
C	Capacitance
c	General control variable
$\hat{c}$	Perturbed control variable
D	Coefficient matrix
D	Diode
D	Average of duty-ratio
D'	Average of complementary duty-ratio, i.e. $D' = 1 - D$
d	Instantaneous duty-ratio
d'	Instantaneous complementary duty-ratio, i.e. $d' = 1 - d$
$\hat{d}$	Perturbed duty-ratio
e_o	Ideal output voltage source
f_s	Switching frequency
G	Set of G-parameters
G_a	Modulator gain factor
G_{cc}	Controller transfer function
G_{ci}	Control-to-input transfer function
G_{co}	Control-to-output transfer function
G_{io}	Input-to-output transfer function
H	Set of H-parameters
H_i	Current measurement gain
h	Element of H-parameter matrix
I	Unit matrix
I	Average current
I_{mpp}	Maximum power point current
I_{pv}	Average photovoltaic current
i	Instantaneous current
i_{SP}	Instantaneous current generated by solar panel
$\hat{i}$	Perturbed current

$\langle i \rangle$	Time averaged current
$\hat{j}$	Perturbed current
L	Inductor
L	Inductance
$L(s)$	Loop gain
$M(D)$	Conversion ratio
m_1	Capacitor voltage on-time slope
m_2	Capacitor voltage off-time slope
Q	Transistor (switch) or flip-flop output
!Q	Negation of flip-flop output
R	Flip-flop reset
R, r	Resistor
R, r	Resistance
r_d	Parasitic resistor of diode (dynamic resistance)
r_{ds}	Parasitic resistor of switch (dynamic resistance)
R_s	Current sensing resistor
r_s	Solar panel series resistance
r_{sh}	Solar panel parallel shunt resistance
S	Flip-flop set
s	Laplace variable, switch
T_{oi}	Output-to-input transfer function
$T_{oi-\infty}$	Ideal output-input transfer function
T_s	Length of switching period
t_{off}	Switch off-time
t_{on}	Switch on-time
$\mathbf{U}$	Input variable vector in Laplace domain
$\mathbf{u}$	Input variable vector in time domain
U	Average voltage
U_{mpp}	Maximum power point voltage
U_{pv}	Average photovoltaic voltage
u	Instantaneous voltage
u_{ctrl}	Output of PID-controller
u_m	Saw-tooth-shaped modulator voltage
u_{meas}	Output of measurement circuit
u_{ref}	Reference voltage

u_{RS}	Voltage drop across sensing resistor
$\hat{u}$	Perturbed voltage
$\langle u \rangle$	Time averaged voltage
$\mathbf{X}$	State variable vector in Laplace domain
$\mathbf{x}$	State variable vector in time domain
$\mathbf{Y}$	Output variable vector in Laplace domain
$\mathbf{y}$	Output variable vector in time domain
Y	Admittance
Y_{in}	Input admittance
Y_o	Output admittance
Y_{SP}	Solar panel source admittance
Z	Impedance
Z_{in}	Input impedance
$Z_{in-\infty}$	Ideal input impedance
Z_o	Output impedance
Δ	Determinant
Ψ	Flux linkage

Subscripts

C	Refers to capacitor
-c	Refers to closed loop
L	Refers to inductor or load
i	Refers to repetition of i times
in	Refers to input
ins	Refers to ideal input energy source
N	Refers to Norton's equivalent
o	Refers to output
-o	Refers to open loop
-oc , oc	Refers to open circuit
off	Refers to switch off-state
on	Refers to switch on-state
-pp	Refers to peak-to-peak value
-sc , sc	Refers to short circuit
S	Refers to energy source
T	Refers to Thevenin's equivalent
d	Refers to diode

Superscripts

-1	Inversed matrix
D	Refers to dual transformation
L	Refers to load affected transfer function
S	Refers to source affected transfer function

Abbreviations

AC	Alternating current
CCM	Continuous conduction mode
DC	Direct current
DCM	Discontinuous conduction mode
KCL	Kirchoff's current law
KVL	Kirchoff's voltage law
MOSFET	Metal-oxide semiconductor field effect transistor
MPP	Maximum power point
MPPT	Maximum power point tracking
PWM	Pulse width modulation
SSA	State-space averaging

1 INTRODUCTION

The use of electrical energy in our daily life is increasing day by day with great pace, which also results in the development of new means of energy generation. Because of the price hike of traditional fossil fuels and climatic changes, the concept of Green Energy is becoming the potential candidate for the new sources of electrical energy generation [1]. Renewable energy sources, e.g. solar cells, solar thermal, wind and biomass, are getting more attention than ever before to fulfil the future energy demands. Electrical energy produced by solar cells is becoming more popular amongst the home users because it is easy to install and it can fulfil the energy needs at small levels without building any big infrastructures.

New developments and the increase in use of photovoltaic (PV) power plants to make the efficient use of sun light brought also the needs of new electronics products which are used to process the produced electrical energy to increase the efficiency. The solar panels generate DC power and are interfaced with a DC-DC converter in order to regulate the output power to the maximum power point, as shown in Fig. 1.1 for the further processing in next stages [2].

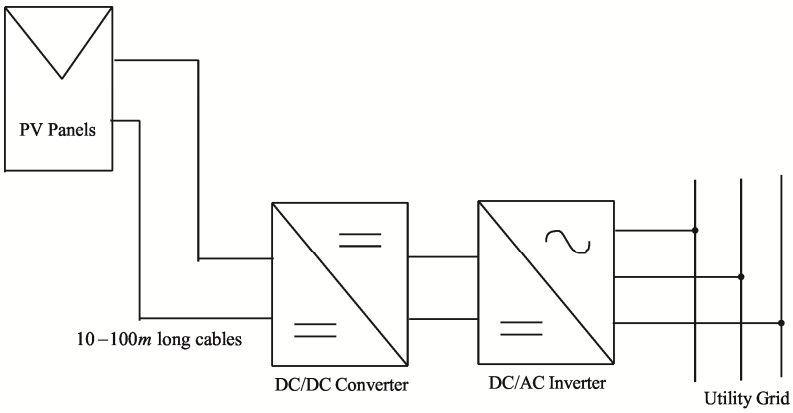

Figure 1.1 *A basic solar power plant topology*

Power converters are classified in two ways, i.e. voltage or current-sourced, depending on their source of energy. Solar panel is considered as a current source and following interfacing power converter in a PV plant should also be a current-sourced converter for a better efficiency [3]. Current-fed converter can be developed by using the duality principle to transform the traditional voltage-fed converter into current-fed converter [3].

The aim of green energy is to reduce the environmental pollution as well as electromagnetic pollution generated by electronics products. The involvement of power electronics devices in photovoltaic systems brought the aspect of electromagnetic interference which could decrease the efficiency of solar panels. The generated EMI may be radiated to atmosphere or conducted through the electronic circuitry paths which may harm the performance of other interconnected system performances. To immune the electronic product from electromagnetic interference, the term Electromagnetic Compatibility (EMC) is used which addresses all the generated noise, regardless of frequency according to the relevant EMC standards [6].

EMI filters are commonly used to reduce the conducted noise emission from the electronic product. While designing EMI filters, two major aspects should be well considered, i.e.

1- The system is electromagnetically compatible to the relevant EMC standards.
2- Stability of the whole system is maintained after insertion of an EMI filter.

EMC standards are not yet available for photovoltaic applications, so, the work in this thesis only focuses on the stability issues when an input EMI filter is added at the interface between the solar panel and current-fed DC/DC converter as shown in Fig. 1.2.

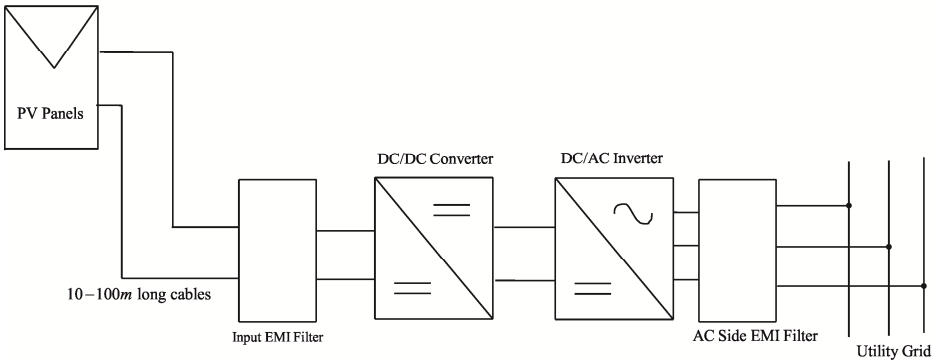

Figure 1.2 *Addition of EMI filters in a PV power plant*

The dynamics of a converter are characterized by its input and output transfer functions [4]. In a cascaded system, as shown in Fig. 1.3, source subsystem effects on all the set of transfer functions of the following stage with a common factor called minor loop gain. Minor loop gain, comprising of output impedance of previous stage and the input impedance of the following stage, defines the stability of the whole system.

The dynamic analysis of the converter is done by using the method of state-space averaging (SSA), previously developed in 1970s by Middlebrook [7]. SSA is a technique to compute different transfer functions of the dc-dc converters which can be used to make the analysis easier. Inductor current and capacitor voltage which are considered to be the state variables and the input and output variables are averaged over a complete

switching period. After proper partial derivatives, the small-signal representation can be obtained by developing proper partial derivatives. A set of transfer functions is then obtained by applying the matrix manipulation technique.

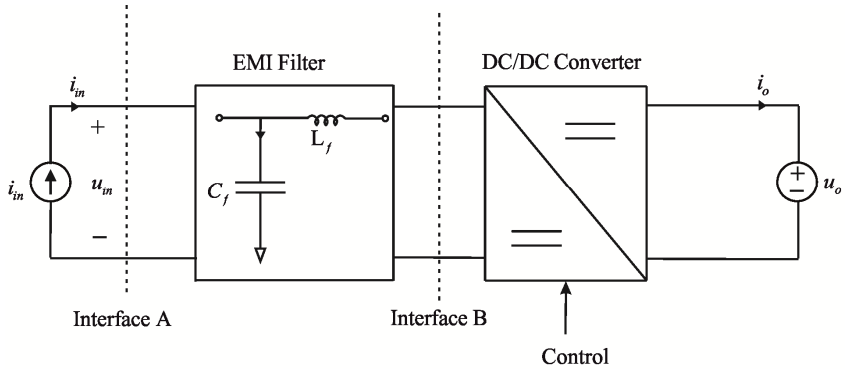

Figure 1.3 *Positions of two interfaces for implementation of control loop*

The output variables are input voltage and output current in current-fed converters and control is implemented from the input voltage. When adding an EMI filter at input, the point at which the control should be implemented is of high interest, i.e. whether before the EMI filter (interface A in Fig. 1.3) or just after the filter (interface B in Fig. 1.3). In this work, the control has been implanted at both of the points separately to check the performance of the system. When the control is implemented at interface A, in Fig. 1.3, the SSA is solved by including the filter in the power stage of the converter, while in other case the SSA is solved for both converter and filter stages separately.

The outline of thesis is as follows. Input EMI filter for photovoltaic power plants and theoretical aspects about the stability of a cascaded system are discussed in Chapter 2. A stability criterion about impedance matching in a cascaded system is briefly described. State-space averaging (SSA) technique to derive the transfer functions of a power converter is discussed in Chapter 3. Different open and closed-loop transfer functions of current-sourced converter and EMI filter are calculated to analyse the stability of the whole system. Symbolic toolbox package from Matlab is used to compute complex transfer functions of the system. In Chapter 4, converter and EMI filter is modelled in Matlab Simulink blocks to verify the validity of the analysed concepts of stability of the whole system. The whole system is modelled by employing different implementations of control loops. Chapter 5 includes the results of the simulations and some concluded remarks are presented in Chapter 6.

2 EMI FILTER FOR PV PLANTS

The idea of Smart Grid to use and generate the electrical energy in an efficient manner is becoming popular nowadays. One of the main source of generating the free energy and utilize in the national grid is solar photovoltaic plants to convert the solar energy into electrical energy. A subsystem of a small PV plant is consisted of solar panels mainly mounted on the roofs which convert solar energy into electrical energy; this generated DC power is further processed using a set of power converter modules.

A typical installation of a photovoltaic subsystem constitutes a power converter module, which consists of a DC/DC converter for maximum power point tracking (MPPT), and a DC/AC inverter to match the utility grid voltage as shown in Fig. 2.1.

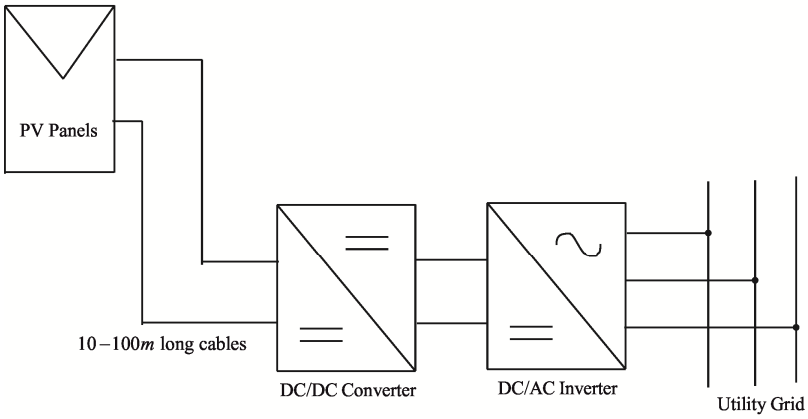

Figure 2.1 *Model of a small PV plant connected with utility grid*

Involvement of the power electronics circuitry may contribute some EMI noise due to the commutation processes at high frequencies involved inside these modules, to the surrounding atmosphere which may cause interference to other devices. The DC side of the PV installation may have long cables which may act as transmitting or receiving antennas for this generated electromagnetic interference [14]. Moreover, since the length of DC line may normally comes into the range of 10 to 100 meters which may act as resonant circuits and can oscillate at several frequencies due to the distributed line longitudinal inductance and transversal capacitances [14]. To overwhelm these problems, an input EMI filter is needed to suppress these kind of noises to the extent of a standardised limits specified by different organizations. To design the EMI filter for DC side of PV applications is still in research process and some tries have been made as discussed in [15]. In this chapter, the basic concept of EMI filter for current-fed DC/DC

converter is discussed and the stability criterion for the cascaded system is also described briefly.

2.1 EMI Filter for current-fed converter

The current-sourced input makes it an ideal converter for the energy sources having current-source nature, because its input voltage is continuous similarly as the input current is continuous in the corresponding voltage-sourced converter [15]. The IV-curve of a photovoltaic panel shows that the following DC/DC converter should be current-sourced instead of voltage-sourced [28]. A current-fed converter is developed by transformation of a voltage-fed converter by applying duality principle [15]. However, a voltage-fed buck converter will act as a current-fed boost as shown in Fig. 2.2.

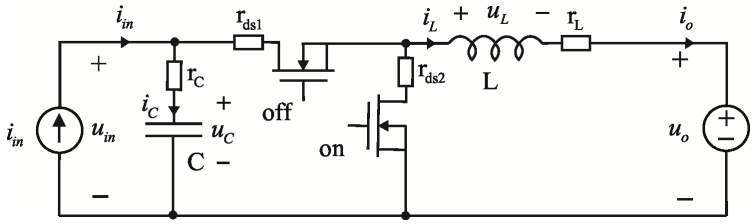

Figure 2.2 *Power stage of current-fed boost DC/DC converter*

A simple EMI filter is composed of a resonance circuit consisting of an inductor and a capacitor. A conventional EMI filter attenuates the voltage signal from its input port and current is attenuated if the signal is coming in from its output port as shown in Fig. 2.3.

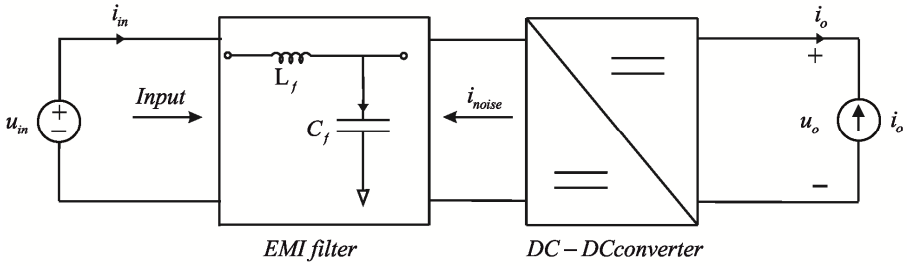

Figure 2.3 *EMI filter for suppression of noise current*

We are dealing with the new converter topology used to interface solar panel, i.e. current-fed converter. In this type of converter noise at the input is in the form of voltage generated by the variations in the current due to switching components which induces voltage across the input line by creating the mutual inductance between two conductors. To reduce this noise voltage an EMI filter is required which can suppress the noise voltage applied at its output port. Filter in Fig. 2.4 is modified using duality principle to achieve this goal.

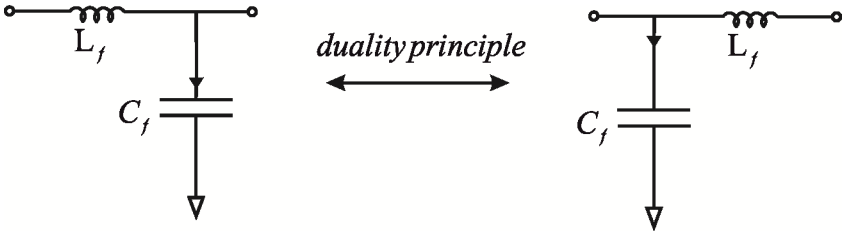

Figure 2.4 *Noise voltage suppression filter drawn from the conventional filter using duality principle*

2.2 Stability of a cascaded system

While designing a system for specific applications, the overall stability of the cascaded system should be treated as an important parameter. The performance of the system depends on the stability of the system. If a system becomes unstable, it may oscillate at some frequencies and may not work properly. When an input EMI filter is needed to install with a power converter, it must be designed in such a way that the stability of the overall cascaded system is not affected to make the proper operation of the converter.

According to the system theory, stability of a cascaded system depends on the output impedance of the first stage and input impedance of the second stage, as shown in Fig. 2.5. To make the operation in a stable region, the impedance matching at the interface of the cascaded system should be achieved. Any mismatch of the impedances may results in a resonant circuit, which may resonate at some specific frequencies.

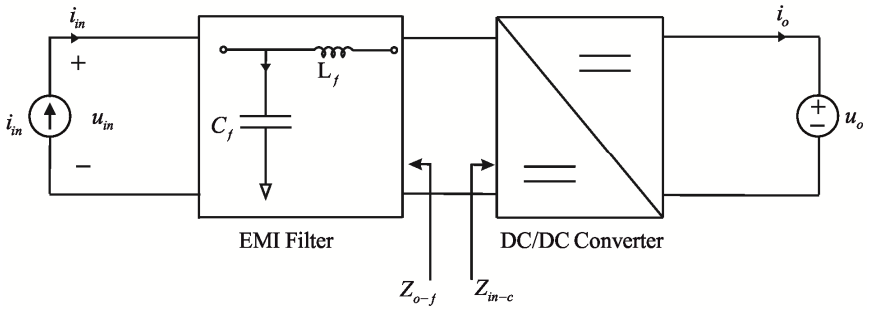

Figure 2.5 *Impedances of two stages at the interface*

From the measurement data, it is revealed that the dynamic resistance of the solar panels changes at different operating points (constant-current region, constant-voltage region and maximum power point). The dynamic resistance of solar penal affects the transfer functions of the filter which results in the change in its output impedance, hence, affecting the dynamics of converter and may cause instability of the whole system at some specific points.

3 MODELING THE WHOLE SYSTEM

Performance analysis of the switched-mode converters is carried out by using dynamic analysis and modeling, which is an important tool to analyse their internal behaviour and working. To make the operation of the converter possible in a smooth and stable way, dynamic modeling is used at the beginning of the converter designing process.

To model a system, different input and output transfer functions are needed to be solved which helps in making the analysis easier. The State-Space Averaging (SSA) is utilized to solve these transfer functions which reveals the dynamics of the system [7] and [34]. The process of state-space averaging is briefly described in three steps as follows,

1. A non-linear average model of switched-mode converter is developed
2. By linearizing the average model at some operating point, a small-signal model is derived
3. By using matrix manipulation, different input and output transfer functions of the switched-mode converter are derived from the small-signal model

These derived transfer functions describe the dynamic behaviour of the converter. On the basis of these transfer functions a two-port model is established. The representations in two-port model are based on Norton's and Thevenin's equivalent circuits [35].

In this chapter, the switched-mode converter and the input EMI filter are analyzed by using the above discussed state-space averaging tool. The used converter is current-sourced and the state-space averaging technique will also be applicable to this converter and filter cascaded system. Input and output dynamics of the source affected converter are described by using control block diagrams.

3.1 State-Space Averaging Technique

The state-space averaging technique is an accurate method to determine the dynamic model of the switched–mode converters which helps in deep analysis of the performance of the system under different conditions. In this section, the main procedure of computing the state-space averaging of the switched-mode converters is discussed. As the EMI filters also comprising of two memory element, so SSA method is also applied to filters to get the accurate dynamic models of the filters which is useful to analyse the effect of various transfer functions on the following converter stage.

There are three sets of variables involved in computing state-space averaging, i.e. state variables (inductor current and capacitor voltages), input and output variables (input and output voltages and currents). These variables are computed separately during on- and off-times. Averaging is performed by multiplying the on time equations with duty ratio *d* and off time equations with complementary duty ratio *d'* and adding both the equation together. These equations can be linearized by taking appropriate partial derivatives to get the small-signal state space [15] and [17].

A set of transfer functions in time domain can be obtained by using the matrix manipulation on the equations given in (3.1), where **u** and **y** denotes input and output variable vectors, respectively **x** denotes the state variable vector. **A**, **B**, **C** and **D** are the coefficient matrices, which consists of different constant elements of the converter circuit, such as inductances *L* and capacitances *C* [15] and [17].

$$\begin{aligned} \frac{d\mathbf{x}(t)}{dt} &= \mathbf{A}\mathbf{x}(t) + \mathbf{B}\mathbf{u}(t) \\ \mathbf{y}(t) &= \mathbf{C}\mathbf{x}(t) + \mathbf{D}\mathbf{u}(t) \end{aligned} \tag{3.1}$$

Frequency domain of the equations in (3.1) can be obtained by using the *Laplace* transformation, as shown in (3.2). By using the matrix manipulation, (3.3) can be found giving the state and output variables from the input variables.

$$\begin{aligned} s\mathbf{X}(s) &= \mathbf{A}\mathbf{X}(s) + \mathbf{B}\mathbf{U}(s) \\ \mathbf{Y}(s) &= \mathbf{C}\mathbf{X}(s) + \mathbf{D}\mathbf{U}(s) \end{aligned} \tag{3.2}$$

$$\begin{aligned} \mathbf{X}(s) &= (s\mathbf{I} - \mathbf{A})^{-1}\mathbf{B}\mathbf{U}(s) \\ \mathbf{Y}(s) &= (\mathbf{C}(s\mathbf{I} - \mathbf{A})^{-1}\mathbf{B} + \mathbf{D})\mathbf{U}(s) \end{aligned} \tag{3.3}$$

From (3.3), the system's transfer functions can be found in matrix $\mathbf{C}(s\mathbf{I} - \mathbf{A})^{-1}\mathbf{B} + \mathbf{D}$. These transfer functions are known as *G*- or *H-parameters* depending on the nature of their input and output variables. In current-sourced converter, these transfer functions are called *H-parameters*.

3.2 H-Parameters

In current sourced converters, the transfer functions are known as H-parameters as shown in (3.4). The dynamics of the converter is described by these parameters. The relationship between input and output variables at open loop is given by,

$$\begin{bmatrix} \hat{u}_{in} \\ \hat{i}_{o} \end{bmatrix} = \begin{bmatrix} Z_{in-o} & T_{oi-o} & G_{ci-o} \\ G_{io-o} & -Y_{o-o} & G_{co-o} \end{bmatrix} \begin{bmatrix} \hat{i}_{in} \\ \hat{u}_{o} \\ \hat{c} \end{bmatrix} \tag{3.4}$$

where $\begin{bmatrix} \hat{i}_{in} & \hat{u}_{o} & \hat{c} \end{bmatrix}^T$ is the input variable vector **U(*s*)**, $\begin{bmatrix} \hat{u}_{in} & \hat{i}_{o} \end{bmatrix}^T$ is the set of output variables denoted by **Y(*s*)** in (3.3). Z_{in-o} is the transfer function which is known as input impedance, T_{oi-o} is denoted by output to input transfer function, G_{ci-o} denotes the control-to-input transfer function, input-to-output transfer function is denoted by G_{io-o}, output admittance is given by transfer function Y_{o-o}, G_{co-o} is denotes the control-to-output transfer function. From (3.4), the output variables can be calculated as shown in (3.5),

$$\begin{aligned} \hat{u}_{in} &= Z_{in-o}\hat{i}_{in} + T_{oi-o}\hat{u}_{o} + G_{ci-o}\hat{c} \\ \hat{i}_{o} &= G_{io}\hat{i}_{in} - Y_{o-o}\hat{u}_{o} + G_{co-o}\hat{c} \end{aligned} \tag{3.5}$$

The same procedure also applies on the current-sourced EMI filter to find the H-parameters for the filter, which are given in (3.6).

$$\begin{bmatrix} \hat{u}_{in} \\ \hat{i}_{o-f} \end{bmatrix} = \begin{bmatrix} Z_{in-f} & T_{oi-f} \\ G_{io-f} & -Y_{o-f} \end{bmatrix} \begin{bmatrix} \hat{i}_{in} \\ \hat{u}_{o-f} \end{bmatrix} \tag{3.6}$$

3.3 Two-Port Model

Switched-mode converters are characterized by using two-port models based on their input sources. A two-port model is used to describe an electrical network with input and output ports, the two-port model is also described as a black box, with input and output ports. Depending on the input and output sources and loads, respectively, different standards are available to describe the system behaviour, i.e. G, H, Z and Y [35].

Conventional voltage-sourced converters are characterized by two-port network model by using the G-parameters. H-parameter model is used to describe the behaviour of current-sourced switched-mode converters, as shown in Fig. 3.1. The input port of the model is Thevinin's equivalent circuit of impedance Z_T and voltage source $\hat{u}_T$.

Output port is the Norton's equivalent circuit consisting of current sink $\hat{j}_N$ and admittance Y_N.

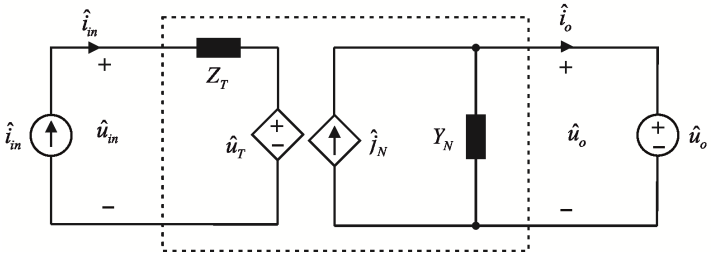

Figure 3.1 *Two-port network model for H-parameter*

The model of current-sourced converter is shown in Fig. 3.2a, using the H-parameters derived in Section 3.2, this model is valid for both at open loop and closed loop. Thevinin's equivalent voltage source is the sum of voltage sources $T_{oi}\hat{u}_o$ and $G_{ci}\hat{c}$, similarly Norton's equivalent current sink is the sum of current sinks $G_{io}\hat{i}_{in}$ and $G_{co}\hat{c}$. Input EMI filter is also modelled in the same way as the current-sourced converter is modelled, with the same H-parameters but at open loop. EMI filter two-port model for this current-fed converter is shown in Fig. 3.2b.

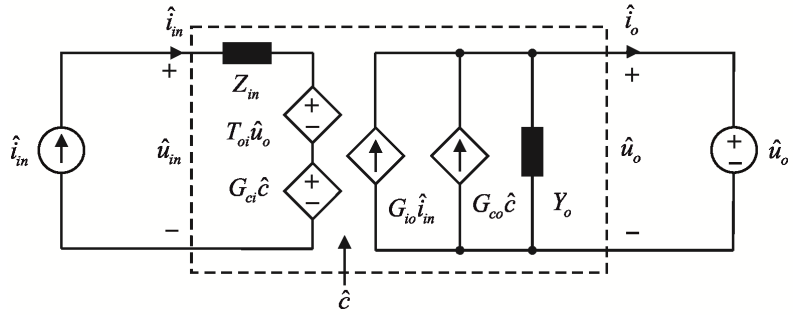

(a)

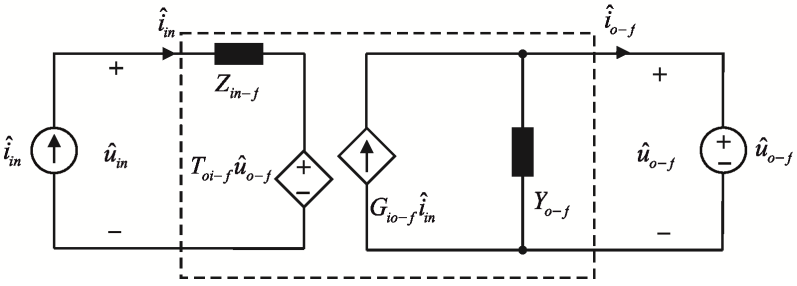

(b)

Figure 3.2 *Two-port models: a) CF-converter b) CF filter*

3.4 Source and Load Effects

In Section 3.3, the two-port models of CF-converter and CF-filter are presented with the ideal voltage and current sources. In reality, source and loads should have some special considerations in the operation of converters, i.e. in CF domain, the current source input admittance Y_s of converter or filter, changes the internal dynamics of the system, similarly, output load impedance Z_L of the voltage source can also affect on the internal dynamics, which in results, changes the behaviour of the overall system. A model of current-fed converter with real source and load is shown in Fig. 3.3,

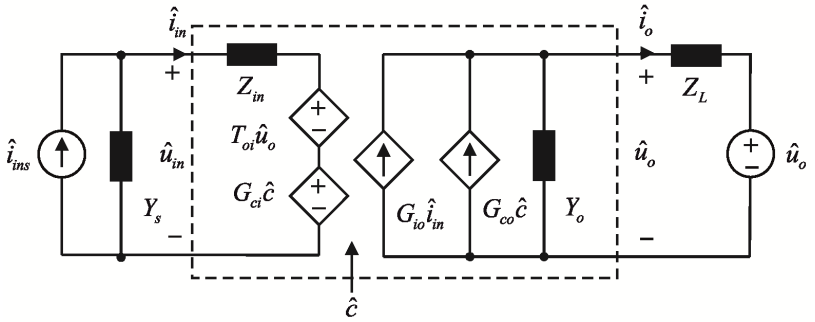

Figure 3.3 *CF-converter model with non-ideal source and load*

The related set of H-parameters of the converter with source and load effects are given in (3.7). Where superscripts 'S' and 'L' denote the source and load effects, respectively, $\hat{i}_{ins}$ is the ideal input current source and $\hat{e}_o$ is the ideal output voltage source.

$$\begin{bmatrix} \hat{u}_{in} \\ \hat{i}_o \end{bmatrix} = \begin{bmatrix} Z_{in}^S & T_{oi}^S & G_{ci}^S \\ G_{io}^S & -Y_o^S & G_{co}^S \end{bmatrix} \begin{bmatrix} \hat{i}_{ins} \\ \hat{u}_o \\ \hat{c} \end{bmatrix}$$
$$\begin{bmatrix} \hat{u}_{in} \\ \hat{i}_o \end{bmatrix} = \begin{bmatrix} Z_{in}^L & T_{oi}^L & G_{ci}^L \\ G_{io}^L & -Y_o^L & G_{co}^L \end{bmatrix} \begin{bmatrix} \hat{i}_{in} \\ \hat{e}_o \\ \hat{c} \end{bmatrix} \tag{3.7}$$

The same rules are implemented for input EMI filter to denote the source effect on its H-parameters and are given in (3.8).

$$\begin{bmatrix} \hat{u}_{in} \\ \hat{i}_{o-f} \end{bmatrix} = \begin{bmatrix} Z_{in-f}^S & T_{oi-f}^S \\ G_{io-f}^S & -Y_{o-f}^S \end{bmatrix} \begin{bmatrix} \hat{i}_{ins} \\ \hat{u}_{o-f} \end{bmatrix} \tag{3.8}$$

As the EMI filter is connected with the current source directly (in our case, solar panels), so first we will find the source effected H-parameters for EMI filter, and using the source-affected output admittance of EMI filter, source-affected H-parameters can be calculated. To find the source-affected H-parameters of EMI filter, $\hat{i}_{in}$ is computed by using KCL in the circuit shown in Fig. 3.4, which is given in (3.9).

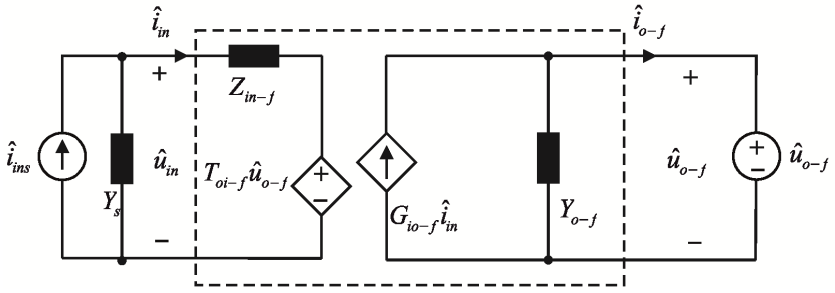

Figure 3.4 *CF filter model with non-ideal source*

$$\hat{i}_{in} = \frac{\hat{i}_{ins} - Y_s T_{oi-f} \hat{u}_{o-f}}{1 + Y_s Z_{in-f}} \tag{3.9}$$

By replacing $\hat{i}_{in}$ in (3.9) with (3.6), gives the source-affected parameters of EMI filter, as shown in (3.10).

$$\begin{bmatrix} Z^S_{in-f} & T^S_{oi-f} \\ G^S_{io-f} & -Y^S_{o-f} \end{bmatrix} = \begin{bmatrix} \dfrac{Z_{in-f}}{1+Y_s Z_{in-f}} & \dfrac{T_{oi-f}}{1+Y_s Z_{in-f}} \\ \dfrac{G_{io-f}}{1+Y_s Z_{in-f}} & -\dfrac{Z_{\text{in-f}-oc} Y_s + 1}{1+Y_s Z_{in-f}} Y^c_{o-f} \end{bmatrix} \tag{3.10}$$

where $Z_{\text{in}-\text{f}-oc}$ is open-circuit input impedance and is given by,

$$Z_{\text{inf}-oc} = \frac{G_{io-f} T_{oi-f}}{Y_{o-f}} + Z_{in-f}$$

Now, the source-affected output admittance of the filter will act as the source admittance for the following stage of the converter, as shown in Fig. 3.5. The source-affected H-parameters for the converter can be found by computing $\hat{i}_{in-conv}$ using the KCL on circuit given in Fig. 3.5, and replacing with $\hat{i}_{in}$ in (3.11) with (3.12), yields the source-affected description of the converter as shown in (3.13).

$$\begin{bmatrix} \hat{u}_{in-conv} \\ \hat{i}_o \end{bmatrix} = \begin{bmatrix} Z^c_{in-conv} & T^c_{oi-conv} & G^c_{ci} \\ G^c_{io-conv} & -Y^c_{o-conv} & G^c_{co} \end{bmatrix} \begin{bmatrix} \hat{i}_{in-conv} \\ \hat{u}_o \end{bmatrix} \tag{3.11}$$

$$\hat{i}_{in-conv} = \frac{\hat{i}_{o-f} - Y_{o-f} T_{oi-conv} \hat{u}_{o-conv} - G_{ci-conv} \hat{c}}{1 + Y_{o-f} Z_{in-conv}} \tag{3.12}$$

$$\begin{bmatrix} \dfrac{Z_{in-con}}{1+Y_{o-f}Z_{in-con}} & \dfrac{T_{oi-con}}{1+Y_{o-f}Z_{in-con}} & \dfrac{G_{ci}}{1+Y_{o-f}Z_{in-con}} \\ \dfrac{G_{io-con}}{1+Y_{o-f}Z_{in-con}} & -\dfrac{1+Z_{in-conv-oc}Y_{o-f}}{1+Y_{o-f}Z_{in-con}} Y_{o-con} & \dfrac{1+Z_{in-con-\infty}Y_{o-f}}{1+Y_{o-f}Z_{in-con}} G_{co} \end{bmatrix} \tag{3.13}$$

where,

$$Z_{in-conv-oc} = \frac{G_{io-conv} T_{oi-conv}}{Y_{o-conv}} + Z_{in-conv}$$

$$Z_{in-conv-\infty} = Z_{in-conv} - \frac{G_{io-conv} G_{ci}}{G_{co}}$$

Load-affected H-parameters of the converter can be found by computing $\hat{u}_o$ from the circuit of Fig. 3.5, and then using (3.11) gives the final set of H-parameters of the converter with effects of load shown in (3.15).

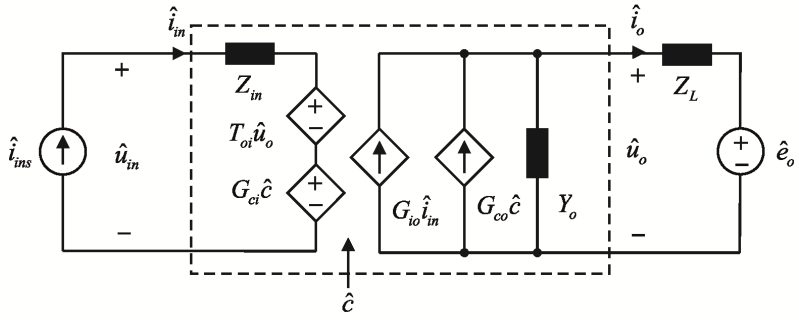

Figure 3.5 *Load-affected CF-converter*

$$\hat{u}_o = \frac{G_{io-conv} Z_L \hat{i}_{in-conv} + \hat{e} + G_{co-conv} Z_L \hat{c}}{1 + Y_o Z_L} \tag{3.14}$$

$$\begin{bmatrix} \hat{u}^L_{in-conv} \\ \hat{i}^L_{o-conv} \end{bmatrix} = \begin{bmatrix} \dfrac{1+Y_{o-conv-sc}Z_L}{1+Y_oZ_L} Z_{in-conv} & \dfrac{T_{oi-conv}}{1+Y_oZ_L} & \dfrac{1+Y_{o-\infty}Z_L}{1+Y_oZ_L} G_{ci} \\ \dfrac{G_{io-conv}}{1+Y_oZ_L} & -\dfrac{Y_{o-conv}}{1+Y_oZ_L} Y^c_{o-conv} & \dfrac{G_{co-conv}}{1+Y_oZ_L} \end{bmatrix} \begin{bmatrix} \hat{i}_{in-conv} \\ \hat{e} \\ \hat{c} \end{bmatrix} \tag{3.15}$$

3.5 Closed-loop Transfer functions

The source and load-affected transfer functions are derived in (3.13) and (3.15), respectively. To derive the closed-loop transfer functions of a source affected converter, a block diagram for a closed loop converter is developed by using (3.5), as shown in Fig. 3.6.

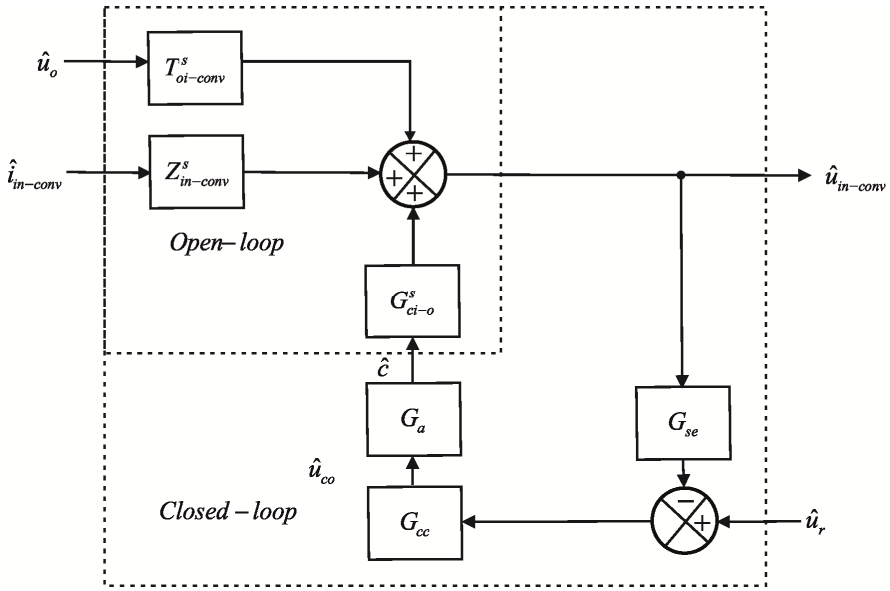

(a)

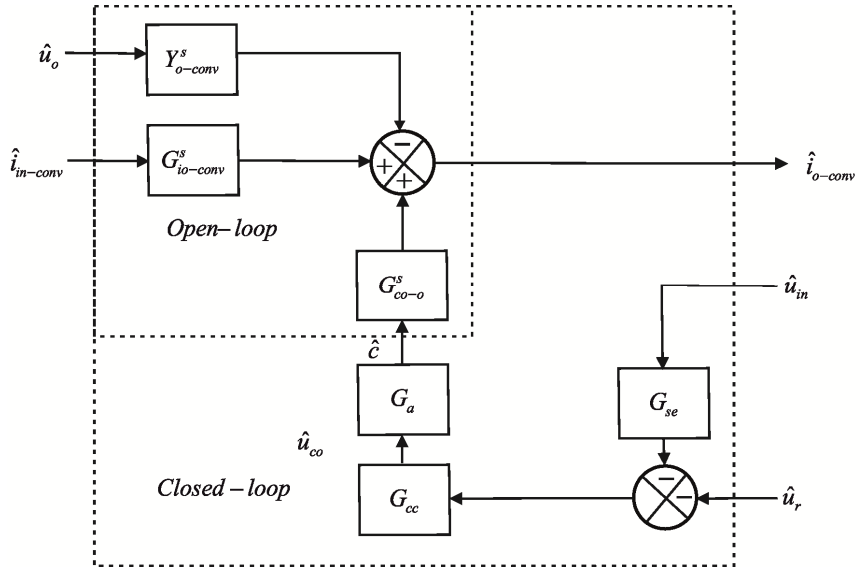

(b)

Figure 3.6 *Closed-loop block diagram of a CF-converter showing (a) output dynamics and (b) Output dynamics*

Using the block diagram given in Fig. 3.6 for output dynamics, the following equations for input voltage and output current can be derived and a set of closed-loop transfer functions can be derived as shown in (3.16).

$$\hat{u}_{in-conv} = \frac{T^s_{oi-conv-o}}{1+L^s_{in-conv}}\hat{u}_o + \frac{Z^s_{in-conv-o}}{1+L^s_{in-conv}}\hat{i}_{in-conv} + \frac{1}{G_{ce}}\frac{L^s_{in-conv}}{1+L^s_{in-conv}}\hat{u}_r$$

$$\hat{i}_o = \left(\frac{G^s_{io-conv-o}}{1+L^s_{in-conv}} + \frac{L^s_{in-conv}}{1+L^s_{in-conv}}G_{io-\infty}\right)\hat{i}_{in-conv} - \left(\frac{Y^s_{o-conv-o}}{1+L^s_{in-conv}} + \frac{L^s_{in-conv}}{1+L^s_{in-conv}}Y^s_{o-\infty}\right)\hat{u}_o + \frac{G^s_{co-o}}{G_{se}G^s_{ci-o}}\frac{L^s_{in-conv}}{1+L^s_{in-conv}}\hat{u}_r$$

where $L^s_{in-conv} = G^s_{ci-conv-o}G_{se}G_{cc}G_a$ is input-voltage loop gain,

$$\begin{bmatrix}\hat{u}^s_{in-conv}\\ \hat{i}^s_{o-conv}\end{bmatrix} = \begin{bmatrix} \dfrac{Z^s_{in-conv-o}}{1+L^s_{in-conv}} & \dfrac{T^s_{oi-conv-o}}{1+L^s_{in-conv}} & \dfrac{1}{G_{ce}}\dfrac{L^s_{in-conv}}{1+L^s_{in-conv}} \\ \dfrac{G^s_{io-conv-o}}{1+L^s_{in-conv}} + \dfrac{L^s_{in-conv}}{1+L^s_{in-conv}}G_{io-\infty} & -\left(\dfrac{Y^s_{o-conv-o}}{1+L^s_{in-conv}} + \dfrac{L^s_{in-conv}}{1+L^s_{in-conv}}Y^s_{o-\infty}\right) & \dfrac{G^s_{co-o}}{G_{se}G^s_{ci-o}}\dfrac{L^s_{in-conv}}{1+L^s_{in-conv}} \end{bmatrix}\begin{bmatrix}\hat{i}_{in-conv}\\ \hat{u}_{o-conv}\\ \hat{u}_r\end{bmatrix} \qquad (3.16)$$

4 SYSTEM LEVEL DYNAMICS

In this chapter, the dynamic modelling of the current-sourced boost converter and input EMI filter are described, respectively. The control method used in the current-sourced boost converter is direct-duty ratio, which is the simplest one. The dynamic modelling of the cascaded system is carried out based on state-space averaging technique, previously described in Chapter 3. The dynamic modelling will give us the desired transfer functions, i.e. the H-parameters, which helps in analysing the performance of the system.

The modelling is done in few steps, depending on the position at which the input control is implemented, as shown in Fig. 4.1. When the control is implemented at 'Position 1' the SSA model is developed for the converter and EMI filter separately, and the effect of the filter is included in the converter's dynamics as described in Chapter 3. Similarly, when the control is taken at 'Position 2' in Fig. 4.1, the EMI filter's power stage is included in the converter's power stage and then a model for the whole system is developed by using SSA technique.

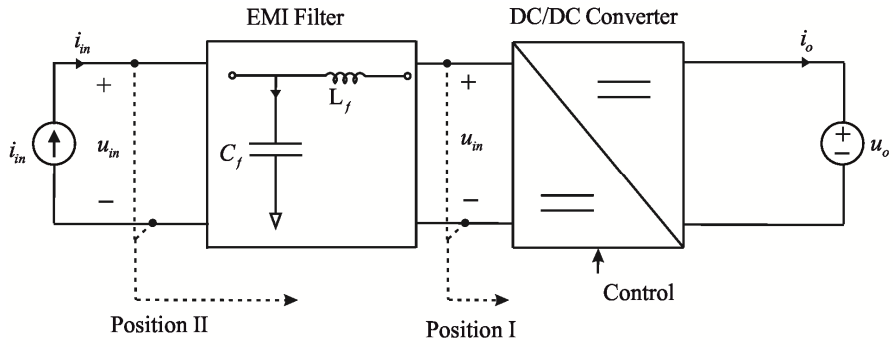

Figure 4.1 *Cascaded-system of DC/DC converter and EMI filter with possibilities of different position for implementation of control.*

4.1 Dynamics of Converter and Filter

When the control is implemented at Position 1 in Fig. 4.1, the transfer functions of both of the converter and filter are derived separately, and then using the source-affected technique discussed in Chapter 3, source-affected H-parameters are derived for the converter.

4.1.1 Transfer Functions of Converter

The parasitic elements also have some impact on the dynamic modelling of the converter. The current-sourced boost converter's power stage with relevant parasitic components is shown in Fig. 4.2. Inductor and capacitor have their relevant parasitic resistors, r_L and r_C as shown in the circuit diagram of Fig. 4.2. The 'on' and 'off' time losses of semiconductor components are also presented in their respective parasitic resistors as r_{ds1} and r_{ds2}.

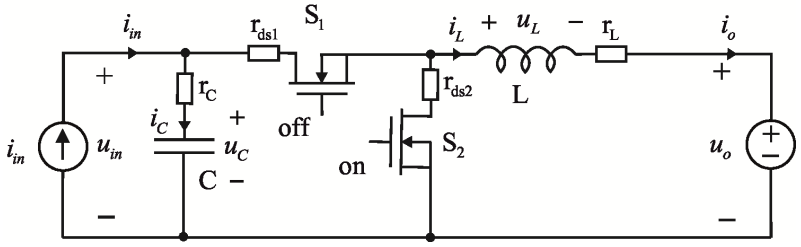

Figure 4.2 *Current-fed boost converter with parasitic elements*

The dynamic modelling is carried out by deriving 'ON time' and 'OFF time' circuits and from these circuits, separate equations for the state variables (capacitor voltage and inductor current) and output variables (input voltage and output current) are solved. Transfer functions are derived by linearizing the derived models.

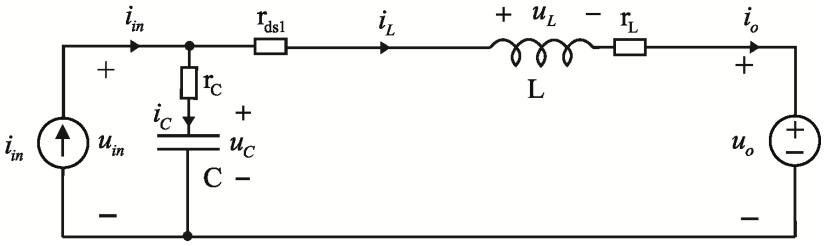

Figure 4.3 *ON-time circuit of CF-boost*

The 'ON time' circuit is shown in Fig. 4.3. The switch S1 is turned ON and switch S2 turned OFF when an inverted gate pulse is applied to the switching components, and the current flows through the switch S1. By applying Kirchoff's laws (KCL and KVL), following equations are derived for capacitor current i_C, inductor voltage u_L, output current i_o and input voltage u_{in}, as shown in (4.1).

$$\begin{aligned} u_L &= u_c - \left(r_c + r_L + r_{ds1}\right) i_L + r_c i_{in} - u_o \\ i_{cf} &= i_{in} - i_L \\ u_{in} &= u_c + r_c i_{in} - r_c i_L \\ i_o &= i_L \end{aligned} \tag{4.1}$$

Similarly, OFF time circuit is shown in Fig. 4.4. The switch S2 is turned ON and S1 is OFF and the current flows through the switch S2.

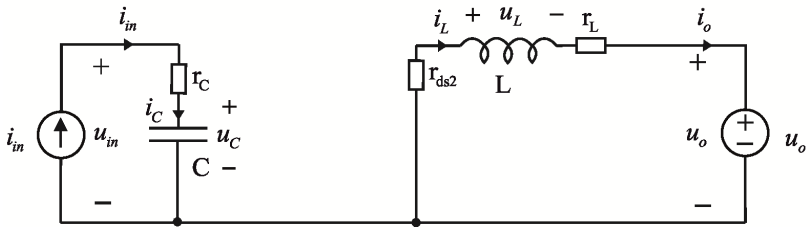

Figure 4.3 *OFF-time circuit of CF-boost*

The voltages and currents of the circuit are computed in (4.2).

$$\begin{aligned} u_L &= -\left(r_L + r_{ds2}\right) i_L - u_o \\ i_c &= i_{in} \\ u_{in} &= u_c + r_c i_{in} \\ i_o &= i_L \end{aligned} \tag{4.2}$$

As discussed in Chapter 3, the state variables are averaged by first computing their derivatives. The ratio of capacitor current and capacitance will give the derivative of the capacitor voltage, as shown in (4.3). Similarly, the ratio of inductor voltage and inductance give the inductor current, given in (4.4).

$$\frac{du_C}{dt} = \frac{i_C}{C} \tag{4.3}$$

$$\frac{di_L}{dt} = \frac{u_L}{L} \tag{4.4}$$

The resulting state-spaces for on- and off-time are given in (4.5) and (4.6).

$$\begin{aligned} \frac{di_L}{dt} = \frac{u_L}{L} &= \frac{u_c}{L} - \frac{\left(r_c + r_L + r_{ds1}\right)}{L} i_L + \frac{r_c}{L} i_{in} - \frac{u_o}{L} \\ \frac{du_C}{dt} = \frac{i_c}{C} &= \frac{i_{in}}{C} - \frac{i_L}{C} \\ u_{in} &= u_c + r_c i_{in} - r_c i_L \\ i_o &= i_L \end{aligned} \tag{4.5}$$

$$\begin{aligned}
&\frac{di_L}{dt} = \frac{u_L}{L} = -\frac{\left(r_L + r_{ds2}\right)}{L} i_L - \frac{u_o}{L} \\
&\frac{du_C}{dt} = \frac{i_c}{C} = \frac{i_{in}}{C} \\
&u_{in} = u_c + r_c i_{in} \\
&i_o = i_L
\end{aligned} \tag{4.6}$$

The averaged state-spaces are computed by multiplying the on-time state-variables in (3.5) with duty ratio *d*, and off-time variables with complementary duty ratio *d'* and adding them together, as shown in (4.7).

$$\begin{aligned}
&\frac{d\left\langle i_L \right\rangle}{dt} = \frac{1}{L}\left\langle u_c \right\rangle - \frac{r_L + d\left(r_c + r_{ds1}\right) + d' r_{ds2}}{L}\left\langle i_L \right\rangle + \frac{dr_c}{L}\left\langle i_{in} \right\rangle - \frac{1}{L}\left\langle u_o \right\rangle \\
&\frac{d\left\langle u_C \right\rangle}{dt} = \frac{1}{C}\left\langle i_{in} \right\rangle - \frac{1}{C}\left\langle i_L \right\rangle \\
&\left\langle u_{in} \right\rangle = \left\langle u_c \right\rangle + r_c \left\langle i_{in} \right\rangle - dr_c \left\langle i_L \right\rangle = \left(1 + r_C C \frac{d}{dt}\right)\left\langle u_C \right\rangle \\
&\left\langle i_o \right\rangle = \left\langle i_L \right\rangle
\end{aligned} \tag{4.7}$$

Change in the averaged capacitor voltages and inductor currents during the switching period has to be zero at steady state. So, the steady-state operating point can be obtained by letting the derivatives in (4.7) equal to zero yielding (4.8).

$$\begin{aligned}
&I_{in} = D' I_L \\
&I_o = I_L = \frac{I_{in}}{D'} \\
&U_{in} = U_C = \frac{U_{in}}{D} + \frac{DD' r_C + r_L + Dr_{ds1} + D' r_{ds2}}{D} I_L
\end{aligned} \tag{4.8}$$

Small-signal state-space can be obtained from (4.7) by developing the proper partial derivatives which gives (4.10). The state-space model is used to compute the H-parameters, which is done by presenting the small-signal state-space in matrix form as shown in (4.10). For simplicity, longer terms can be reduced by using extra variables, as shown below,

$$\begin{aligned}
&R_1 = r_L + D\left(r_c + r_{ds1}\right) + D' r_{ds2} \\
&R_2 = (D' r_C + r_{ds1} - r_{ds2}) I_L - U_C
\end{aligned}$$

$$\begin{bmatrix} \frac{d\hat{i}_L}{dt} \\ \frac{d\hat{u}_c}{dt} \end{bmatrix} = \begin{bmatrix} -\frac{R_1}{L} & \frac{D}{L} \\ -\frac{D}{C} & 0 \end{bmatrix} \begin{bmatrix} \hat{i}_L \\ \hat{u}_c \end{bmatrix} + \begin{bmatrix} \frac{Dr_C}{L} & -\frac{1}{L} & -\frac{R_2}{L} \\ \frac{1}{C} & 0 & -\frac{I_L}{C} \end{bmatrix} \begin{bmatrix} \hat{i}_{in} \\ \hat{u}_o \\ \hat{d} \end{bmatrix}$$
$$\begin{bmatrix} \hat{u}_{in} \\ \hat{i}_o \end{bmatrix} = \begin{bmatrix} 0 & 1+r_cC\frac{d}{dt} \\ 1 & 0 \end{bmatrix} \begin{bmatrix} \hat{i}_L \\ \hat{u}_c \end{bmatrix} + \begin{bmatrix} 0 & 0 & 0 \\ 0 & 0 & 0 \end{bmatrix} \begin{bmatrix} \hat{i}_{in} \\ \hat{u}_o \\ \hat{d} \end{bmatrix} \quad (4.10)$$

The derivation of H-parameters is carried out from the matrices obtained in (4.10) in Laplace domain by using proper software packages such as Matlab Symbolic toolbox. The obtained open-loop transfer functions are presented as follows,

Set of computed H-parameters are too long which can be splited into denominator and numerator, as shown in (4.11). The denominator is the determinant of the computed transfer functions which is a common term in all H-parameters.

$$\begin{bmatrix} Z_{in-o} & T_{oi-o} & G_{ci-o} \\ G_{io-o} & -Y_{o-o} & G_{co-o} \end{bmatrix} = \frac{\begin{bmatrix} h_{11} & h_{12} & h_{13} \\ h_{21} & -h_{22} & h_{23} \end{bmatrix}}{\Delta} \quad (4.11)$$

4.1.1.1 Determinant:

$$\Delta = s^2 + s\frac{D(r_c + r_{ds1}) + D'r_{ds2} + r_L}{L} + \frac{D^2}{LC} \quad (4.12)$$

4.1.1.2 Input Dynamics:

$$h_{11} = \Delta Z_{in-o} = \left(\frac{s}{C} + \frac{DD'r_c + Dr_{ds1} + D'r_{ds2} + r_L}{LC}\right)(1 + sr_cC)$$

$$h_{12} = \Delta T_{oi-o} = \frac{D}{LC}(1 + sr_cC)$$

$$h_{13} = \Delta G_{ci-o} = -\left(s\frac{I_L}{C} + \frac{(D^2r_c + r_{ds2} + r_L)I_L + DU_C}{LC}\right)(1 + sr_cC)$$

4.1.1.3 Output Dynamics:

$$h_{21} = \Delta G_{io-o} = \frac{D}{LC}(1 + sr_c C)$$

$$h_{22} = \Delta Y_{o-o} = \frac{s}{L}$$

$$h_{23} = \Delta G_{co-o} = -\left(\frac{(r_{ds1} - r_{ds2} + D' r_C) I_L - U_C}{L} + \frac{D I_L}{LC} \right)$$

4.1.2 Transfer Functions of EMI Filter

The set of transfer functions for the input EMI filter (H-parameteres) can also be computed by using the state-space averaging technique, because an EMI filter is also composed of memory elements (inductors and capacitors). The power stage of a current sourced EMI filter is shown in Fig. 4.4.

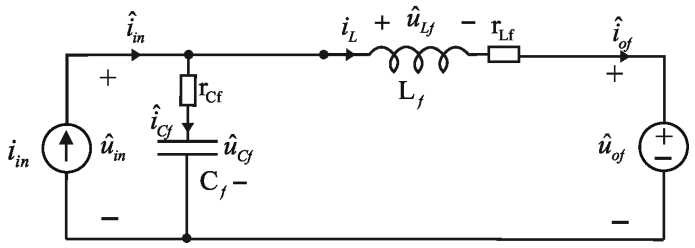

Figure 4.4 *Power stage of current-sourced EMI filter*

Using Kirchoff's laws, the equations for inductor voltage, capacitor current, and output variables are derived, as shown in (4.13).

$$\begin{aligned}
u_{Lf} &= \frac{di_{Lf}}{dt} = \frac{u_{cf}}{L_f} - \frac{\left(r_{cf} + r_{Lf}\right)}{L_f} i_{Lf} + \frac{r_{cf}}{L_f} i_{in} - \frac{u_{of}}{L_f} \\
i_{cf} &= \frac{du_{cf}}{dt} = \frac{i_{in}}{C_f} - \frac{i_{Lf}}{C_f} \\
u_{in} &= u_{cf} + r_{cf} - r_{cf} i_{Lf} = \left(1 + r_{cf} C_f \frac{d}{dt}\right) u_{cf} \\
i_{of} &= i_{Lf}
\end{aligned} \tag{4.13}$$

The obtained state-space can be presented in matrix form which yields (4.14).

$$\begin{bmatrix} \frac{di_{Lf}}{dt} \\ \frac{du_{cf}}{dt} \end{bmatrix} = \begin{bmatrix} -\frac{r_{Lf}+r_{cf}}{L_f} & \frac{1}{L_f} \\ -\frac{1}{C_f} & 0 \end{bmatrix} \begin{bmatrix} i_{Lf} \\ u_{cf} \end{bmatrix} + \begin{bmatrix} -\frac{1}{L_f} & \frac{r_{cf}}{L_f} \\ 0 & \frac{1}{C_f} \end{bmatrix} \begin{bmatrix} i_{in} \\ u_{of} \end{bmatrix}$$
$$\begin{bmatrix} u_{in} \\ i_{of} \end{bmatrix} = \begin{bmatrix} 0 & 1+r_{cf}C_f s \\ 1 & 0 \end{bmatrix} \begin{bmatrix} i_{Lf} \\ u_{cf} \end{bmatrix} + \begin{bmatrix} 0 & 0 \\ 0 & 0 \end{bmatrix} \begin{bmatrix} i_{in} \\ u_{of} \end{bmatrix} \quad (4.14)$$

Matlab symbolic toolbox is used to compute the transfer functions from matrix manipulation. The set of H-parameters for EMI filter is shown in (4.15).

$$\begin{bmatrix} \hat{u}_{in} \\ \hat{i}_{of} \end{bmatrix} = \begin{bmatrix} Z_{in-f} & T_{oi-f} \\ G_{io-f} & -Y_{o-f} \end{bmatrix} \begin{bmatrix} \hat{i}_{in} \\ \hat{u}_{o-f} \end{bmatrix} \quad (4.15)$$

4.1.2.1 Dynamics of filter:

$$Z_{\text{in}-f} = \left(\frac{(C_f L_f r_{cf})s^2 + (L_f + C_f r_{Lf} r_{cf})s + r_{Lf}}{(C_f L_f)s^2 + (C_f r_{Lf} + C_f r_{cf})s + 1} \right)$$

$$T_{oi-f} = \frac{(1 + s r_{cf} C_f)}{(C_f L_f)s^2 + (C_f r_{Lf} + C_f r_{cf})s + 1}$$

$$G_{io-f} = \frac{(1 + s r_{cf} C_f)}{(C_f L_f)s^2 + (C_f r_{Lf} + C_f r_{cf})s + 1}$$

$$Y_{o-f} = \left(\frac{sC_f}{(C_f L_f)s^2 + (C_f r_{Lf} + C_f r_{cf})s + 1} \right)$$

4.1.3 Effect of Solar panel and EMI filter on Converter:

As briefly described in Chapter 3, the dynamic resistance of the solar panel affects the EMI filter dynamics which results in a slight change in the response of the H-parameters. The dynamic resistance of the solar cell changes with the change in its operating point, so have different effects on different operating regions (constant current region, constant voltage region and maximum power point). The measurement was taken in the Department of Electrical Energy Engineering Power Electronics lab which shows response of dynamic resistance of the solar panel is shown in Fig. 4.5.

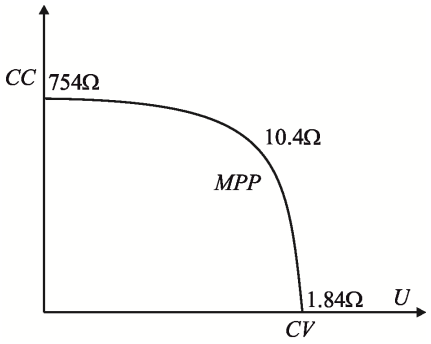

Figure 4.5 *Solar cell dynamic resistance measured values at different operating regions (constant current, constant voltage and MPP)*

The source-affected transfer functions of EMI filter affects the dynamical behaviour of the converter, as a result instability may occur. The output admittance of the filter is the main candidate (See Section 3.4) for affecting the current-sourced converter, as shown in Fig. 4.6.

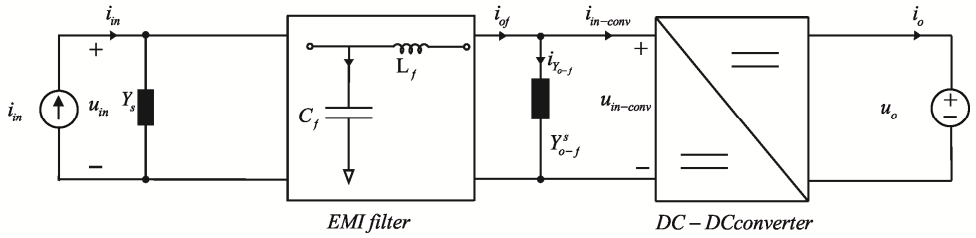

Figure 4.6 *Source admittances of solar panel and EMI filter which affects on converter dynamics*

The output admittance of filter and the input impedance of converter both form a new term known as ‘minor loop gain’ which is present in every transfer function of the converter as shown in (3.13). This defined minor loop gain tells the stability of the converter and its different transfer functions. The minor loop gain is shown in (4.16).

$$\text{minor loop gain} = Z_{in-con}Y_{o-f} \tag{4.16}$$

4.1.4 Transfer Functions of both converter and filter together

When the control loop is implemented at ‘position 1’ in Fig. 4.1, the modelling of the system is carried out by using the filter in the power stage of the converter as shown in Fig. 4.7. This system includes two inductors and two capacitors, therefore, will be solved for four state variables, i.e. u_{Lf} u_L i_C and i_{Cf}. Where u_{Lf} is the filter inductor voltage, u_L is the converter inductor voltage, i_C is the converter capacitor current and

i_{Cf} is the filter capacitor current. The parasitic elements also have some impact on the dynamic modelling of the converter. The overall power stage of filter and converter with relevant parasitic components are shown in Fig. 4.7. Converter inductor '*L*' and capacitor '*C*' have their relevant parasitic resistors, r_L and r_C , similarly filter inductor ' L_f 'and capacitor ' C_f ' have their relevant parasitic resistors, r_{Lf} and r_{Cf} . The 'on' and 'off' time losses of semiconductor components are also presented in their respective parasitic resistors as r_{ds1} and r_{ds2} .

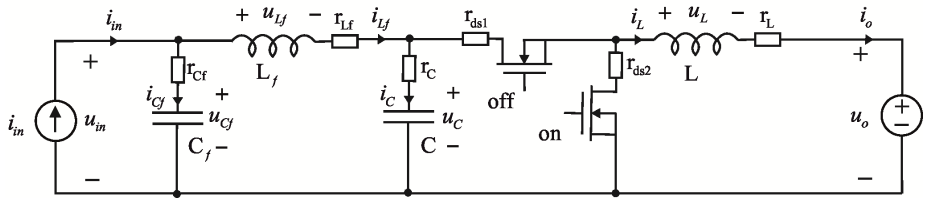

Figure 4.7 *The overall power stage of CF-converter and EMI filter*

The dynamic modelling is carried out by deriving 'ON time' and 'OFF time' circuits and from these circuits, separate equations for the state variables (capacitor voltages u_{cf} u_C and inductor currents i_{Lf} , i_L) and output variables (input voltage and output current) are solved. Transfer functions are derived by linearizing the derived models.

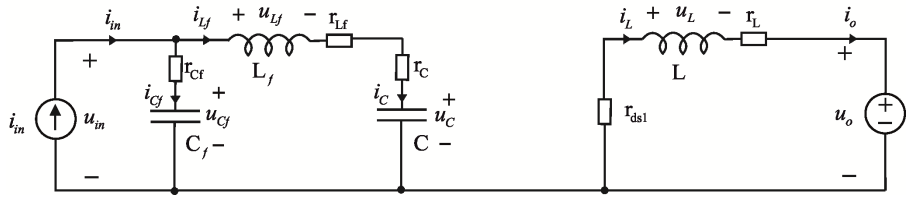

Figure 4.8 *ON-time circuit of CF-boost*

The 'ON time' circuit is shown in Fig. 4.8. The switch S1 is turned ON and switch S2 turned OFF when an inverted gate pulse is applied to the switching components, and the current flows through the switch S1. By applying Kirchoff's laws (KCL and KVL), following equations are derived for capacitor current i_C, inductor voltage u_L, output current i_o and input voltage u_{in}, as shown in (4.17).

$$
\begin{aligned}
u_{Lf} &= u_{cf} - u_c + (r_{cf} + r_{Lf} + r_c) i_{Lf} + r_{cf} i_{in} \\
u_L &= -(r_L + r_{ds1}) i_L - u_o \\
i_{cf} &= i_{in} - i_{Lf} \\
i_c &= i_{Lf} \\
u_{in} &= u_{cf} + r_{cf} i_{cf} = (1 + r_{cf} C_f \frac{d}{dt}) u_{cf} \\
i_o &= i_L
\end{aligned}
\tag{4.17}
$$

Similarly, OFF time circuit is shown in Fig. 4.9. The switch S2 is turned ON and S1 is OFF and the current flows through the switch S2.

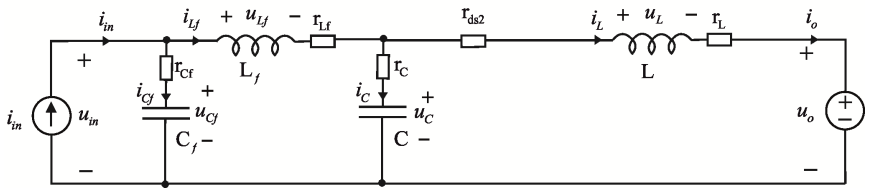

Figure 4.9 *OFF-time circuit.*

The voltages and currents of the circuit are computed in (4.18).

$$
\begin{aligned}
u_{Lf} &= u_{cf} - u_c - (r_{cf} + r_{Lf} + r_c) i_{Lf} + r_{cf} i_{in} + r_c i_L \\
u_L &= u_c - u_o + r_c i_{Lf} - (r_L + r_c + r_{ds1}) i_L \\
i_{cf} &= i_{in} - i_{Lf} \\
i_c &= i_{Lf} - i_L \\
u_{in} &= u_{cf} + r_{cf} i_{cf} = (1 + r_{cf} C_f \frac{d}{dt}) u_{cf} \\
i_o &= i_L
\end{aligned}
\tag{4.18}
$$

As discussed in Chapter 3, the state variables are averaged by first computing their derivatives. The ratio of capacitor currents and capacitance will give the derivative of the capacitor voltage, as shown in (4.19). Similarly, the ratio of inductor voltage and inductance give the inductor current, given in (4.20).

$$
\frac{du_C}{dt} = \frac{i_C}{C} \Rightarrow i_C = C \frac{du_C}{dt} \tag{4.19}
$$

$$
\frac{di_L}{dt} = \frac{u_L}{L} \Rightarrow u_L = L \frac{di_L}{dt} \tag{4.20}
$$

The resulting state-spaces for on- and off-time are given in (4.21) and (4.22).

$$
\begin{aligned}
&\frac{di_{Lf}}{dt}=\frac{u_{Lf}}{L_f}=\frac{u_{cf}}{L_f}-\frac{u_c}{L_f}+\frac{(r_{cf}+r_{Lf}+r_c)}{L_f}i_{Lf}+\frac{r_{cf}}{L_f}i_{in}\\
&\frac{di_L}{dt}=\frac{u_L}{L}=-\frac{(r_L+r_{ds1})}{L}i_L-\frac{u_o}{L}\\
&\frac{du_{cf}}{dt}=\frac{i_{cf}}{C_f}=\frac{i_{in}}{C_f}-\frac{i_{Lf}}{C_f}\\
&\frac{du_c}{dt}=\frac{i_c}{C}=\frac{i_{Lf}}{C}\\
&u_{in}=u_{cf}+r_{cf}i_{cf}=(1+r_{cf}C_f\frac{d}{dt})u_{cf}\\
&i_o=i_L
\end{aligned}
\tag{4.21}
$$

$$
\begin{aligned}
&\frac{di_{Lf}}{dt}=\frac{u_{Lf}}{L_f}=\frac{u_{cf}}{L_f}-\frac{u_c}{L_f}-\frac{(r_{cf}+r_{Lf}+r_c)}{L_f}i_{Lf}+\frac{r_{cf}}{L_f}i_{in}+\frac{r_c}{L_f}i_L\\
&\frac{di_L}{dt}=\frac{u_L}{L}=\frac{u_c}{L}-\frac{u_o}{L}+\frac{r_c}{L}i_{Lf}-\frac{(r_L+r_c+r_{ds1})}{L}i_L\\
&\frac{du_{cf}}{dt}=\frac{i_{cf}}{C_f}=\frac{i_{in}}{C_f}-\frac{i_{Lf}}{C_f}\\
&\frac{du_c}{dt}=\frac{i_c}{C}=\frac{i_{Lf}}{C}-\frac{i_L}{C}\\
&u_{in}=u_{cf}+r_{cf}i_{cf}=(1+r_{cf}C_f\frac{d}{dt})u_{cf}\\
&i_o=i_L
\end{aligned}
\tag{4.22}
$$

The averaged state-spaces are computed by multiplying the on-time state-variables in (3.5) with duty ratio *d*, and off-time variables with complementary duty ratio *d'* and adding them together, as shown in (4.23).

$$
\begin{aligned}
&\frac{d\left\langle u_{Cf}\right\rangle}{dt}=\frac{1}{C_f}\left\langle i_{in}\right\rangle-\frac{1}{C_f}\left\langle i_{Lf}\right\rangle\\
&\frac{d\left\langle u_{C}\right\rangle}{dt}=\frac{1}{C}\left\langle i_{Lf}\right\rangle-\frac{d'}{C}\left\langle i_{L}\right\rangle\\
&\frac{d\left\langle i_{L_f}\right\rangle}{dt}=\frac{1}{L_f}\left\langle u_{cf}\right\rangle-\frac{1}{L_f}\left\langle u_{c}\right\rangle-\frac{r_{cf}+r_c+r_{Lf}}{L_f}\left\langle i_{Lf}\right\rangle+\frac{r_{cf}}{L_f}\left\langle i_{in}\right\rangle+\frac{d'r_c}{L_f}\left\langle i_{L}\right\rangle\\
&\frac{d\left\langle i_{L}\right\rangle}{dt}=\frac{d'}{L}\left\langle u_{c}\right\rangle-\frac{1}{L}\left\langle u_{o}\right\rangle+\frac{d'r_c}{L}\left\langle i_{Lf}\right\rangle-\frac{(r_L+dr_{ds1}+d'(r_{ds2}+r_c))}{L}\left\langle i_{L}\right\rangle\\
&\left\langle u_{in}\right\rangle=\left\langle u_{cf}\right\rangle+r_{cf}\left\langle i_{in}\right\rangle-dr_{cf}\left\langle i_{Lf}\right\rangle=\left(1+r_{Cf}C_f\frac{d}{dt}\right)\left\langle u_{Cf}\right\rangle\\
&\left\langle i_{o}\right\rangle=\left\langle i_{L}\right\rangle
\end{aligned}
\tag{4.23}
$$

Change in the averaged capacitor voltages and inductor currents during the switching period have to be zero at steady state. So, the steady-state operating point can be obtained by letting the derivatives in (4.23) equal to zero yielding (4.24).

$$
\begin{aligned}
&I_{in}=I_{Lf}\\
&I_o=I_L\Rightarrow I_o=\frac{I_{in}}{D'}\\
&I_{Lf}=D'I_L\\
&U_C=U_{Cf}-r_{Lf}I_{in}\\
&U_{in}=U_{Cf}=\frac{U_o}{D'}+\frac{D'^2(r_{Lf}+r_L)+Dr_{ds1}+D'(r_{ds2}-r_C)+r_L}{D'^2}I_{in}
\end{aligned}
\tag{4.24}
$$

Small-signal state-space can be obtained from (4.23) by developing the proper partial derivatives which gives (4.25).

$$
\begin{aligned}
&\frac{d\hat{u}_{Cf}}{dt}=\frac{1}{C_f}\hat{i}_{in}-\frac{1}{C}\hat{i}_{Lf}\\
&\frac{d\hat{u}_{C}}{dt}=\frac{1}{C}\hat{i}_{Lf}-\frac{D'}{C}\hat{i}_{L}-\frac{I_L}{C}\hat{d}\\
&\frac{d\hat{i}_{Lf}}{dt}=\frac{\hat{u}_{cf}}{L_f}-\frac{\hat{u}_{c}}{L_f}+\frac{r_{cf}}{L_f}\hat{i}_{in}-\frac{(r_{cf}+r_c+r_{Lf})}{L_f}\hat{i}_{Lf}+\frac{D'r_c}{L_f}\hat{i}_{L}-\frac{r_cI_L}{L_f}\hat{d}\\
&\frac{d\hat{i}_{L}}{dt}=\frac{D'\hat{u}_{c}}{L}-\frac{\hat{u}_{o}}{L}+\frac{D'r_c}{L}\hat{i}_{Lf}-\frac{r_L+Dr_{ds1}+D'(r_{ds2}+r_c)}{L}\hat{i}_{L}\\
&\qquad-\frac{(-r_C+r_{ds1}-r_{ds2})I_L+r_cI_{Lf}-U_C}{L}\hat{d}\\
&\hat{u}_{in}=(1+sr_{Cf}C_f)\hat{u}_{Cf}\\
&\hat{i}_{o}=\hat{i}_{L}
\end{aligned}
\tag{4.25}
$$

The state-space model is used to derive the H-parameters, which is done by presenting the small-signal state-space in matrix form, as shown in (4.26). For simplicity, longer terms can be reduced by using extra variables, as shown below,

$$
\begin{aligned}
R_1 &= r_L + Dr_{ds1} + D'\left(r_c + r_{ds2}\right) \\
R_2 &= r_{Lf}r_L + r_L r_{cf} + r_L r_c + D'r_c^2 - \frac{D'^2 L}{L_f}r_c^2 + D'r_{Lf}r_c + Dr_{Lf}r_{ds1} + D'r_{Lf}r_{ds2} \\
&\quad + D'r_{cf}r_c + Dr_{cf}r_{ds1} + Dr_c r_{ds1} + D'r_{cf}r_{ds2} + D'r_c r_{ds2} + \frac{DD'r_L}{C} \\
R_3 &= r_{Lf} + r_L + r_{cf} + r_c \\
R_4 &= r_L + D'^2 r_c + D'r_c + Dr_{ds1} + D'r_{ds2} - DD'r_c \\
R_5 &= (r_{cf}^2 + r_{Lf}r_{cf} + r_L r_{cf} + r_{cf}r_c + D'r_f r_c + Dr_{cf}r_{ds1} + D'r_{cf}r_{ds2} \\
R_6 &= r_{Lf} + r_L + r_{cf} + r_c + D'r_c + Dr_{ds1} + D'r_{ds2} \\
U_1 &= (r_{ds1} - r_{ds2} - r_C)I_L + r_C I_{Lf} + U_C
\end{aligned}
$$

$$
\begin{bmatrix} \frac{d\hat{u}_{cf}}{dt} \\ \frac{d\hat{u}_c}{dt} \\ \frac{d\hat{i}_{Lf}}{dt} \\ \frac{d\hat{i}_L}{dt} \end{bmatrix} = \begin{bmatrix} 0 & 0 & -\frac{1}{C_f} & 0 \\ 0 & 0 & \frac{1}{C} & -\frac{D}{C} \\ \frac{1}{L_f} & -\frac{1}{L_f} & -\frac{r_{Lf}+r_{cf}+r_c}{L} & \frac{D'r_c}{L} \\ 0 & \frac{D}{L_f} & \frac{D'r_c}{L} & -\frac{R_1}{L} \end{bmatrix} \begin{bmatrix} \hat{u}_{cf} \\ \hat{u}_c \\ \hat{i}_{Lf} \\ \hat{i}_L \end{bmatrix} + \begin{bmatrix} \frac{1}{C_f} & 0 & 0 \\ 0 & 0 & \frac{I_L}{C} \\ \frac{r_{cf}}{L_f} & 0 & \frac{r_c I_L}{L_f} \\ 0 & -\frac{1}{L} & -\frac{R_2}{L} \end{bmatrix} \begin{bmatrix} \hat{i}_{in} \\ \hat{u}_o \\ \hat{d} \end{bmatrix} \tag{4.26}
$$

$$
\begin{bmatrix} \hat{u}_{in} \\ \hat{i}_o \end{bmatrix} = \begin{bmatrix} 1+sr_{cf}C_f & 0 & 0 & 0 \\ 0 & 0 & 0 & 1 \end{bmatrix} \left[\begin{bmatrix} \hat{u}_{cf} \\ \hat{u}_c \\ \hat{i}_{Lf} \\ \hat{i}_L \end{bmatrix} \right] + \begin{bmatrix} 0 & 0 & 0 \\ 0 & 0 & 0 \end{bmatrix} \begin{bmatrix} \hat{i}_{in} \\ \hat{u}_o \\ \hat{d} \end{bmatrix}
$$

The derivation of H-parameters is carried out from the matrices obtained in (4.26) in Laplace domain by using proper software packages such as Matlab Symbolic toolbox. The obtained open-loop transfer functions are presented as follows;

Set of computed H-parameters are too long which can be splitted into denominator and numerator, as shown in (4.11). The denominator is the determinant of the computed transfer functions which is a common term in all H-parameters.

$$\begin{bmatrix} Z_{in-o} & T_{oi-o} & G_{ci-o} \\ G_{io-o} & -Y_{o-o} & G_{co-o} \end{bmatrix} = \frac{\begin{bmatrix} h_{11} & h_{12} & h_{13} \\ h_{21} & -h_{22} & h_{23} \end{bmatrix}}{\Delta} \tag{4.11}$$

4.1.4.1 Determinant:

$$\begin{aligned}\Delta = {} & s^4 C_f C L_f L^2 + s^3 (C_f C L_f L R_3 + C_f C D' L_f L r_c + C_f C D L_f L r_{ds1} + \\ & C_f C D' L_f L r_{ds2}) + s^3 (C_f L^2 + C L^2 + C_f C L_f R_2 + s^2 (C_f L R_4 + C L (D' r_c + D r_{ds1} \\ & + D' r_{ds2}) + C_f L_f D D' (r_{Lf} + r_{cf} + r_c) + s D D' L\end{aligned}$$

4.1.4.2 Input Dynamics:

$$\begin{aligned}h_{11} = \Delta Z_{in-o} = {} & s^4 (C_f C L_f L^2 r_{cf}) + s^3 (C L_f L^2 - C_f C L^2 r_{cf}^2 + C_f C L_f L R_5) + s^2 (L^2 r_{cf} (C_f - C) \\ & + C L_f L + C_f C r_L r_{cf}^2 (L_f - L) R_6 + C_f C (L_f (r_{Lf} r_L r_{cf} + r_L r_{cf} r_c + D' r_{cf} r_c^2 + D' r_{cf}^2 r_c \\ & + D r_{cf}^2 r_{ds1} + D' r_{Lf} r_{cf} r_c \\ & + D r_{Lf} r_{cf} r_{ds1} + D' r_{Lf} r_{cf} r_{ds2} + r_{cf} r_c r_{ds1} + D' r_{cf} r_c r_{ds2}) + L (D' r_{cf}^2 r_c \\ & - D'^2 r_{cf} r_c^2 - D r_{cf}^2 r_{ds1} - D' r_{cf}^2 r_{ds2}))) + s (L^2 + C L_f (D' r_c^2 + r_{Lf} r_L \\ & + r_L r_{cf} + r_L r_c + D' r_{Lf} r_c + D r_{Lf} r_{ds1} + D' r_{Lf} r_{ds2} + D r_{cf} r_{ds1} + D r_c r_{ds1} \\ & + D' r_{cf} r_{ds2} + D' r_c r_{ds2}) + C_f L (r_L r_{cf} + D' r_c r_{cf} + D r_{ds1} r_{cf} + D' r_{cf} r_{ds2} \\ & - D D' r_{Lf} r_{cf} - D D' r_{cf} r_c) - C L (D'^2 r_c^2 + D' r_{cf} r_c + D r_{cf} r_{ds1} + D' r_{cf} r_{ds2}) \\ & + D D' L_f L + C_f L_f D D' (r_{cf}^2 + r_{Lf} r_{cf} + r_{cf} r_c)) + L (r_L + D' r_c + D r_{ds1} + D' r_{ds2} \\ & - D'^2 r_c - D D' r_{cf} - D D' r_c) + D D' L_f (r_{Lf} + r_{cf} + r_c)\end{aligned}$$

$$h_{12} = \Delta T_{oi-o} = s^2 (C_f C D' L r_{cf} r_c) + s (C_f D L r_{cf} + C D' L r_c) + D L$$

$$\begin{aligned}h_{13} = \Delta G_{ci-o} = {} & s^3 (-C_f C I_L L^2 r_{cf} r_c) + s^2 (I_L L (L C_f r_{cf} - L C r_c - C_f C r_{cf} r_c (2 D' r_c \\ & - r_L - D r_{ds1} + D' r_{ds1} - 2 D' r_{ds2})) + D' C_f C r_{cf} r_c L I_{Lf}) + s (I_L L (L \\ & + C_f r_L r_{cf} - C r_L r_c - 2 C D' r_c^2 - C_f r_{cf} r_c + D' C_f r_{cf} r_c + 2 D C_f r_{cf} (2 r_{ds1} \\ & - r_{ds2}) + D' C_f r_{cf} r_{ds2} - C r_c (D r_{ds1} - D' r_{ds1} - 2 D' r_{ds2}) - C_f D'^2 r_{cf} r_c \\ & - D D' C_f r_c r_{cf}) + I_{Lf} L r_c (D' C r_c + D C_f r_{cf}) + U_c L (D C_f r_{cf} + D' C r_c)) \\ & + (I_L L (r_L - D'^2 r_c - D r_c + D' r_c + 2 D r_{ds1} - D r_{ds2} + D' r_{ds2} - D D' r_c) \\ & + D L U_c + D I_{Lf} L r_c)\end{aligned}$$

4.1.4.3 Output Dynamics:

$$h_{21} = \Delta G_{io-o} = s^2(C_f CD'Lr_{cf}r_c) + s(C_f D'Lr_{cf} + CD'Lr_c) + D'L$$

$$h_{22} = \Delta Y_{o-o} = s^3(-C_f CL_f L) + s^2(-C_f CL_f(r_{Lf} - r_{cf} - r_c) + s(-C_f L - CL)$$

$$\begin{aligned} h_{23} = \Delta G_{co-o} = {} & s^3(C_f CL_f L(U_c - I_L(r_c - r_{ds1} + r_{ds2}) + I_{Lf}r_c)) + s^2(C_f CL_f(I_{Lf}r_c^2 \\ & - I_L r_c^2 + U_c(r_{Lf} + r_{cf} + r_c) + I_{Lf}r_c(r_{Lf} + r_{cf}) + I_L(r_{Lf}(r_c + r_{ds1} - r_{ds2}) \\ & + r_{cf}(r_c + r_{ds1} - r_{ds2}) + r_c(r_{ds1} - r_{ds2}))) + C_f CLD'I_L r_c^2 - C_f LL_f D'I_L) \\ & + s(C_f L(U_c + I_{Lf}r_c - I_L(r_c - r_{ds1} + r_{ds2})) + CL(I_L(-r_c + r_{ds1} - r_{ds2}) \\ & + I_{Lf}r_c) - C_f L_f I_L D'(r_{Lf} + r_{cf} + r_c))) - D'LI_L \end{aligned}$$

5 SIMULATION RESULTS

Simulations give a smooth way to design a project in a precise and efficient manner. In this thesis work, the main work is to verify the analysed concepts with the help of simulations. There might be some problems in the design which can bring the variations in the estimated results. However, simulation before finalising the design can avoid such mistakes and become helpful to tackle the problems in the design.

Matlab Simulink is used to build the simulation models which are based on the dynamical modelling of the systems, discussed in Chapter 4. The bode diagrams of various transfer functions to verify the stability of the system and the frequency response simulations are presented in this chapter. The frequency responses of transfer functions are evaluated by using a pre-defined Matlab script at some specific frequency. The simulink models are built separately for CF-converter and EMI filter when the control is implemented just before the converter. Similarly, a model is created for the case when control is taken before the filter.

5.1 Simulink Model for CF-Converter and EMI Filter

5.1.1 Case I

Simulations are done by using the Matlab Simulink models. The switching converter is modelled by using its on- and off-time circuits and a duty ratio is implemented to get a switching simulink model. The model for EMI filter is constructed simply by using its circuit presented in Chapter 4. In first case, both the converter and filter are modelled separately, with the input voltage of filter and the converter inductor current are the output variables of the whole system. The overall constructed model is shown in Fig. 5.1.

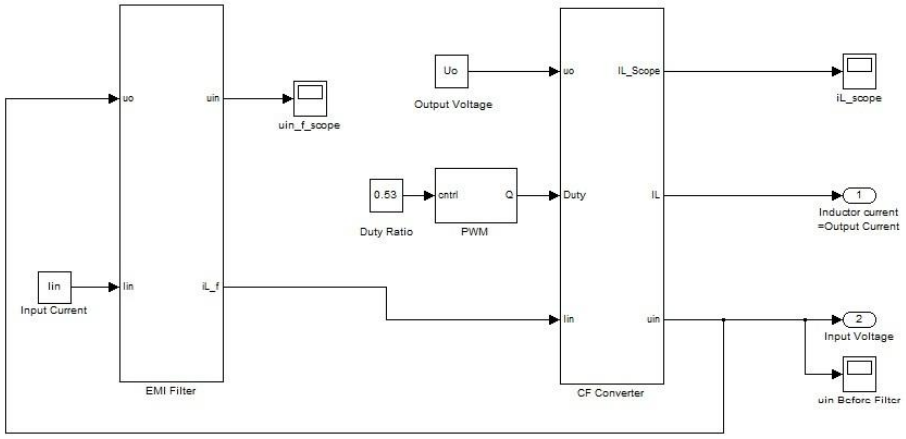

Figure 5.1 *Simulink model of the whole system*

There are three sub-blocks involved in the model of Fig.5.1. Model of EMI filter is shown in Fig. 5.2, this model is built by using the circuit diagram of Fig. 4.3. two output variables, u_{in} and i_o , are computed as shown in Fig. 5.2.

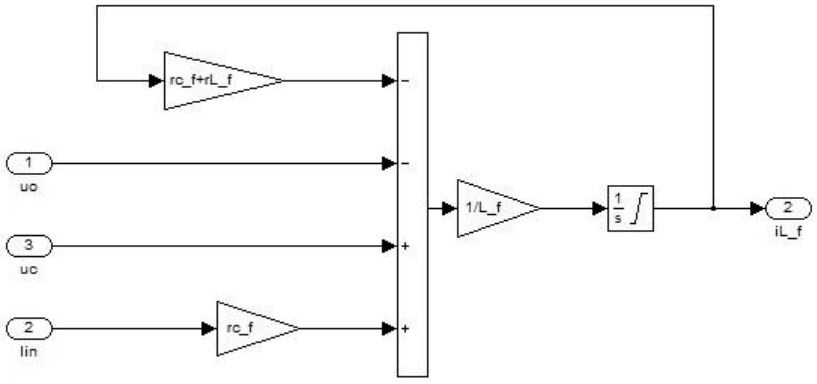

(a)

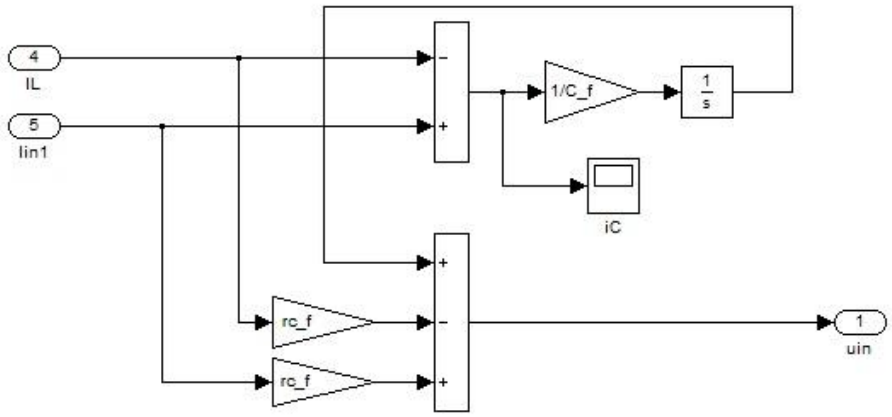

(b)

Figure 5.2 *EMI filter blocks; (a) output current and (b) input voltage*

PWM simulink block is shown in Fig. 5.3. It controls the input voltage by using direct-duty ratio control method. Gate signals of the switch used in converter are controlled by using this block.

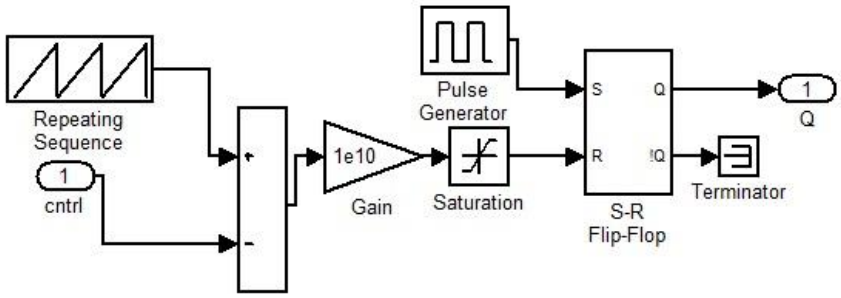

Figure 5.3 *PWM Simulink block to control the gate signal*

Fig. 5.4 gives a preview of the different blocks of the switching converter to compute the state variables and output variables. State and output variables are calculated by using the algorithm developed by using the on- and off-time circuit diagrams of the converter. The algorithm is given in (5.1), where q and $\overline{q}$ are the on-time and off-time functions of the duty ratio, respectively.

$$\frac{dy}{dt} = q\left[\text{on-time equations}\right] + \overline{q}\left[\text{off-time equations}\right] \tag{5.1}$$

Using the algorithm shown in (5.2), the block for inductor current is developed which is shown in Fig. 5.4.

$$\frac{di_L}{dt} = q\left[\frac{u_c}{L} - \frac{(r_c + r_L + r_{ds1})}{L} i_L + \frac{r_c}{L} i_{in} - \frac{u_o}{L}\right] + \bar{q}\left[-\frac{(r_L + r_{ds2})}{L} i_L - \frac{u_o}{L}\right] \tag{5.2}$$

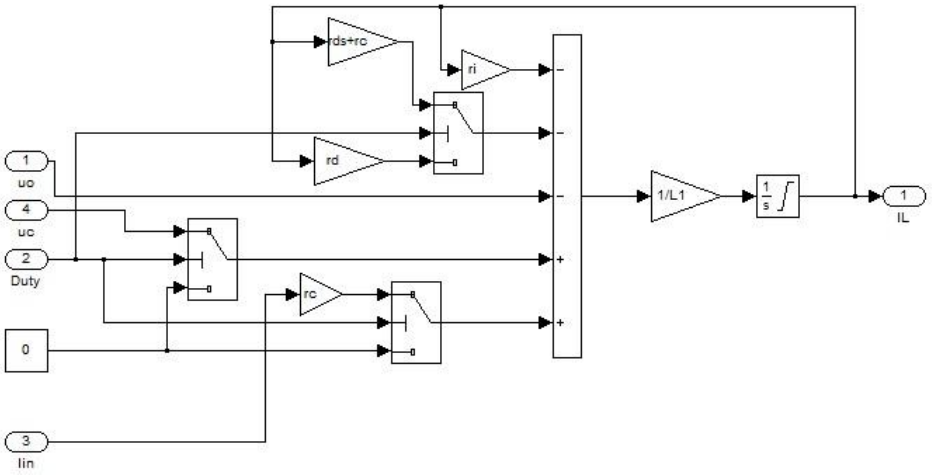

Figure 5.4 *Inductor current* i_L

Fig. 5.5 shows the input voltage of the converter which is developed from the algorithm given in (5.3).

$$u_{in} = q\left[u_c + r_c i_{in} - r_c i_L\right] + \bar{q}\left[u_c + r_c i_{in}\right] \tag{5.3}$$

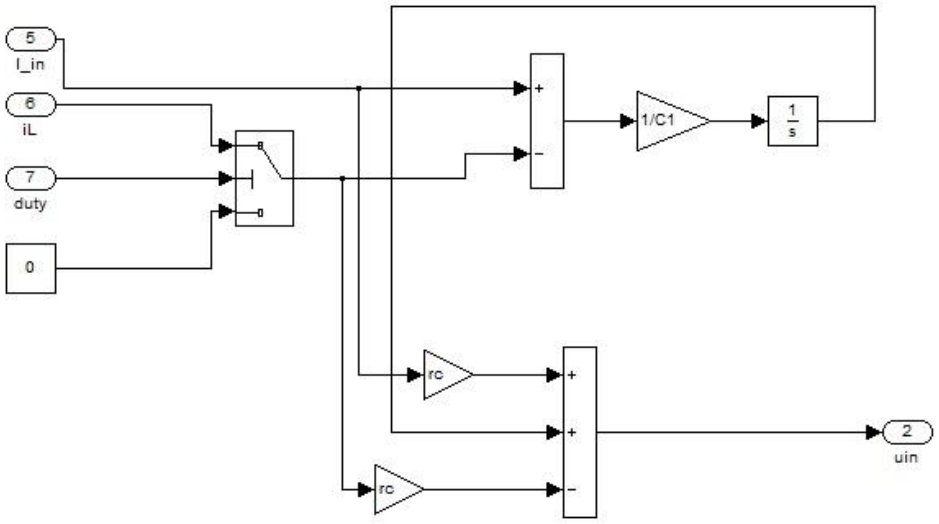

Figure 5.5 *Input voltage* u_{in}

5.1.2 Case II

A simulink model is developed to check the stability of the system when the control of the converter is implemented as shown in Fig. 5.6. In such a case, the input filter is considered in the power stage of the converter, and the dynamics of the system can be evaluated by solving the whole system altogether (See Chapter 4).

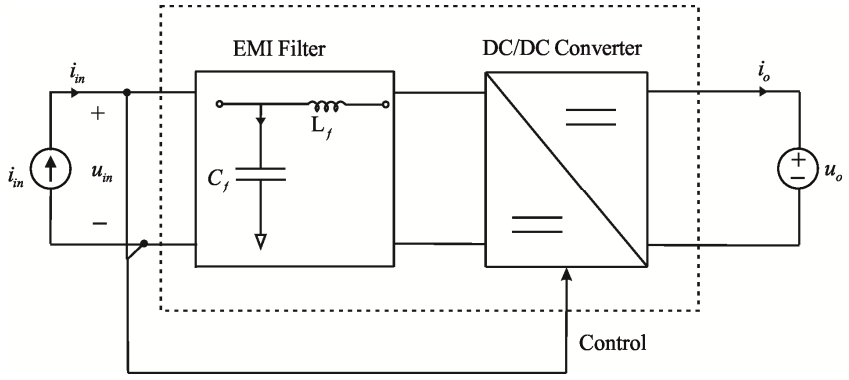

Figure 5.6 *implementation of the control before EMI filter*

The block diagram of simulink model is shown in Fig. 5.7, consists of different sub-blocks. This model includes two inductor currents (filter inductor current i_{Lf} and converter inductor current i_L) and two capacitor voltages (filter capacitor voltage u_{cf} and converter capacitor voltage u_c), which are calculated by using on- and off-time circuits of the power stage. Output variable, output current is equal to the converter inductor current and input voltage is equal to the filter capacitor voltage.

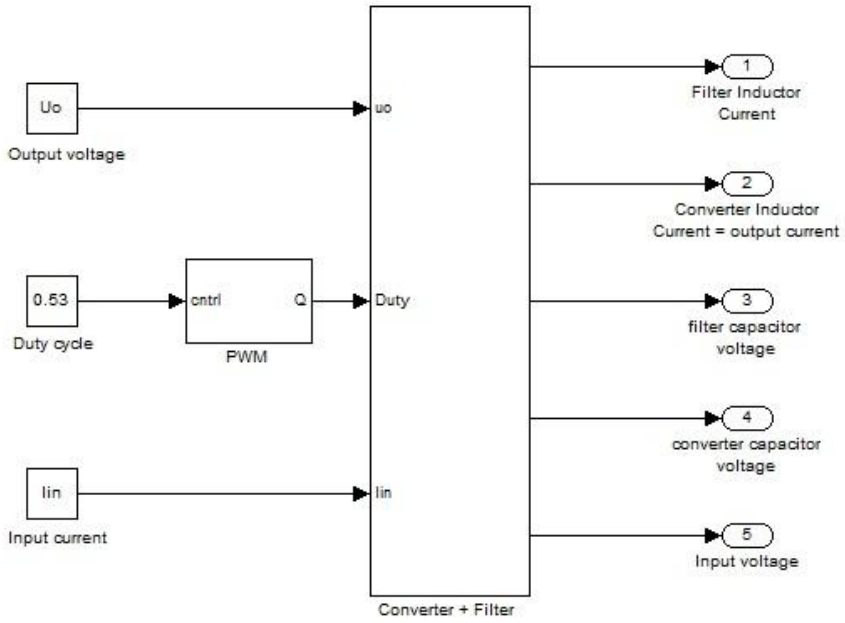

Figure 5.7 *Converter and filter simulink block at open loop*

State and output variables are calculated as separate subblocks, as shown in Fig. 5.8. Each subblock represents the state and output variables.

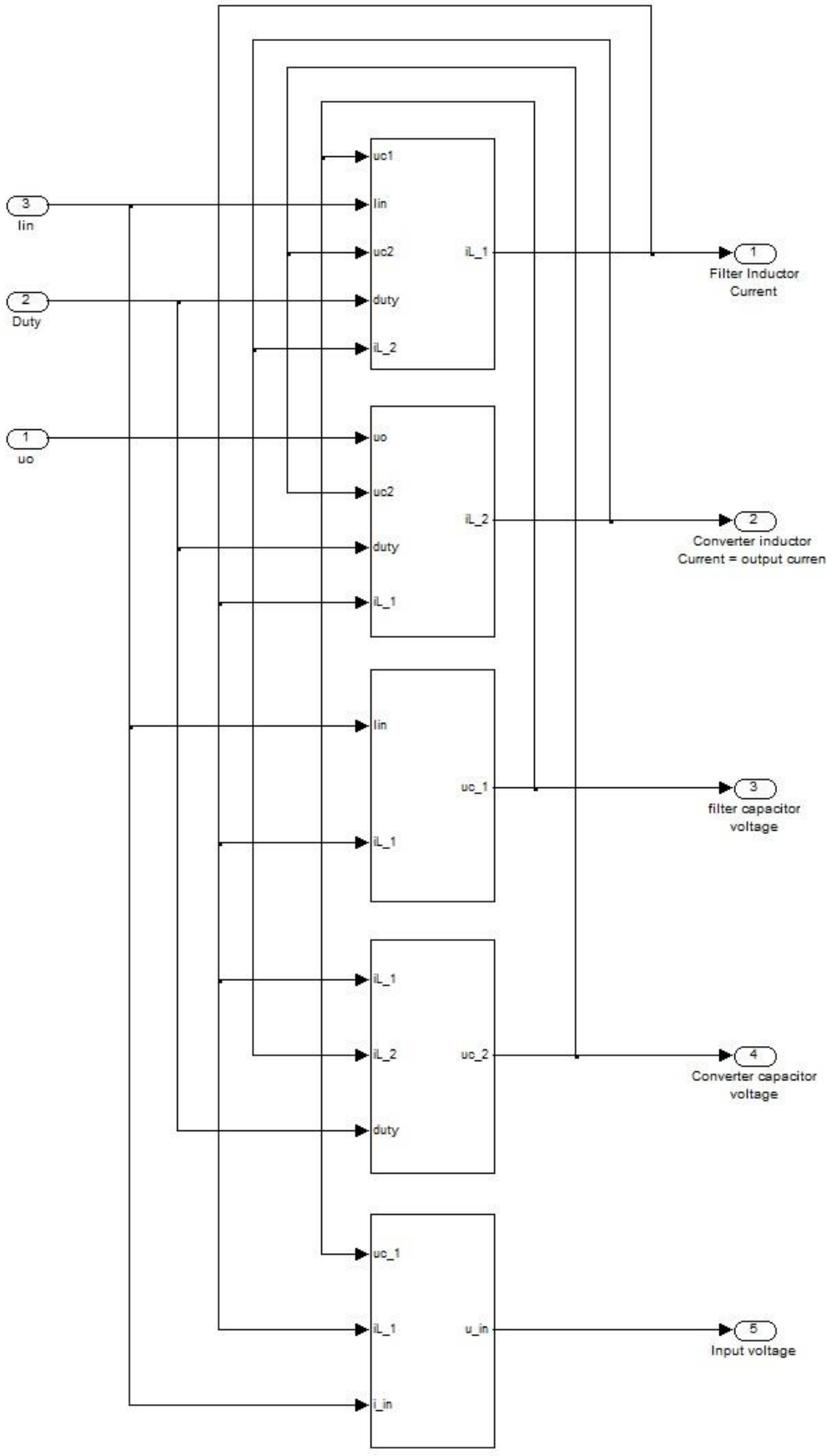

Figure 5.8 *State and output variables of the whole system*

State and output variables are calculated by using the algorithm developed by using the on- and off-time circuit diagrams of the converter. The algorithm is given in (5.1), where q and $\overline{q}$ are the on-time and off-time functions of the duty ratio, respectively.

$$\begin{aligned}\frac{di_{Lf}}{dt} &= q\left[\frac{u_{cf}}{L_f}-\frac{u_c}{L_f}+\frac{(r_{cf}+r_{Lf}+r_c)}{L_f}i_{Lf}+\frac{r_{cf}}{L_f}i_{in}\right] \\ &+\overline{q}\left[\frac{u_{cf}}{L_f}-\frac{u_c}{L_f}-\frac{(r_{cf}+r_{Lf}+r_c)}{L_f}i_{Lf}+\frac{r_{cf}}{L_f}i_{in}+\frac{r_c}{L_f}i_L\right]\end{aligned} \tag{5.4}$$

Fig. 5.9 shows the subblock of filter inductor current, developed from the algorithm given in (5.4).

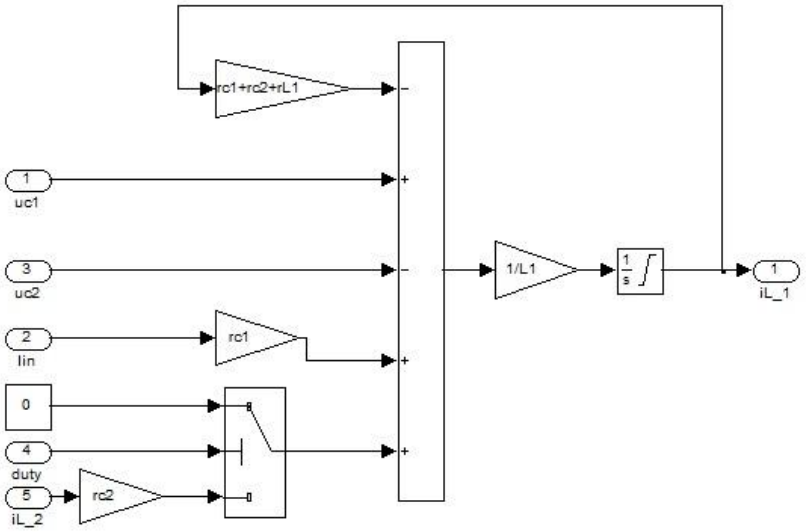

Figure 5.9 *Simulink block of filter inductor current*

Fig. 5.10 shows the subblock of filter inductor current, developed from the algorithm given in (5.5).

$$\begin{aligned}\frac{di_L}{dt} &= q\left[-\frac{(r_L+r_{ds1})}{L}i_L-\frac{u_o}{L}\right] \\ &+\overline{q}\left[\frac{u_c}{L}-\frac{u_o}{L}+\frac{r_c}{L}i_{Lf}-\frac{(r_L+r_c+r_{ds1})}{L}i_L\right]\end{aligned} \tag{5.5}$$

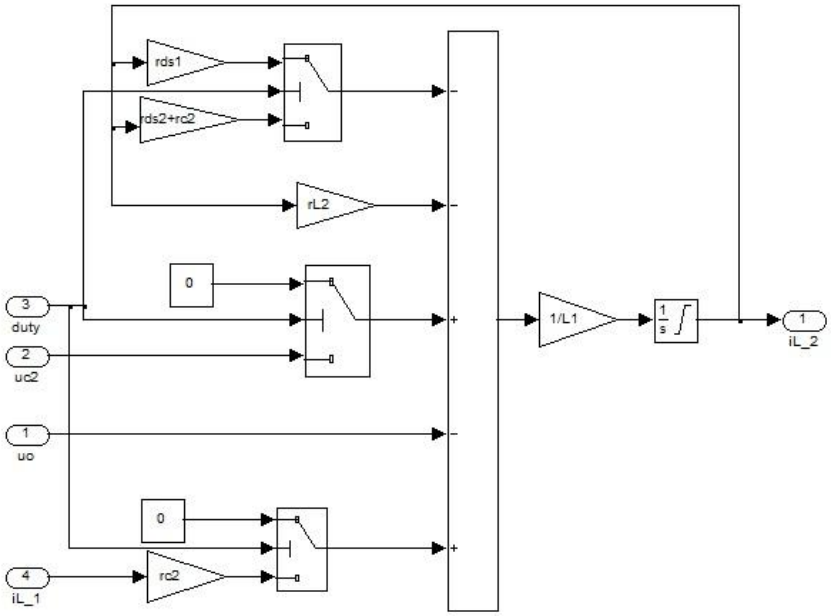

Figure 5.10 Simulink block of converter inductor current

Fig. 5.11 shows the subblock of filter capacitor voltage, developed from the algorithm given in (5.6).

$$u_{cf} = q\left[\frac{i_{in}}{C_f} - \frac{i_{Lf}}{C_f}\right] + \overline{q}\left[\frac{i_{in}}{C_f} - \frac{i_{Lf}}{C_f}\right] \tag{5.6}$$

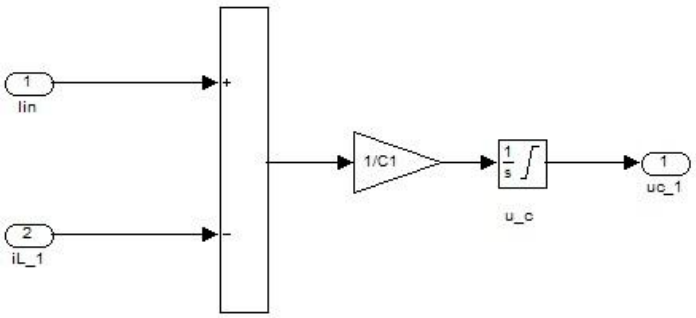

Figure 5.11 *Simulink sub block of filter capacitor voltage*

Fig. 5.12 shows the subblock of filter capacitor voltage, developed from the algorithm given in (5.7).

$$u_c = q\left[\frac{i_{Lf}}{C}\right] + \overline{q}\left[\frac{i_{Lf}}{C} - \frac{i_L}{C}\right] \tag{5.7}$$

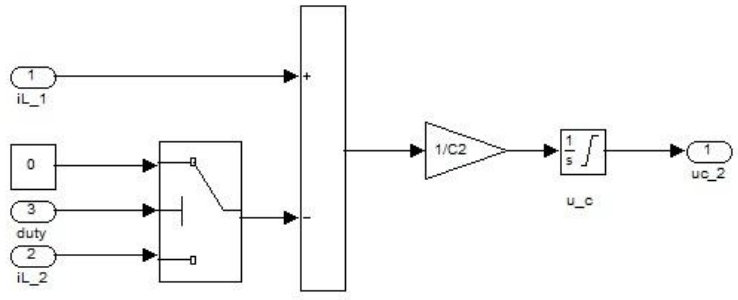

Figure 5.12 Simulink model for converter capacitor voltage

Fig. 5.13 shows the subblock of filter capacitor voltage, developed from the algorithm given in (5.8).

$$u_{in} = q\left[u_{cf} + r_{cf} i_{in} - r_{cf} i_{Lf}\right] + \overline{q}\left[u_{cf} + r_{cf} i_{in} - r_{cf} i_{Lf}\right] \tag{5.7}$$

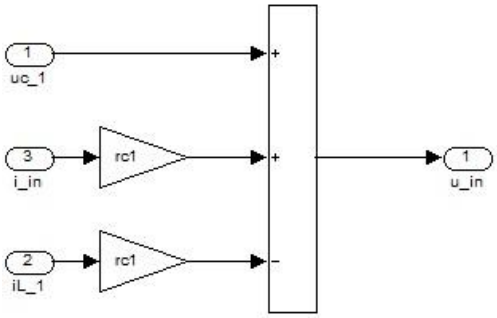

Figure 5.13 *Input voltage simulation block*

5.2 Verifications with Simulations

The work done in this thesis is verified with suitable simulations using Matlab Simulink for building simulation models. The components and specifications for switching converter used in the simulations are taken from [3]. The filter components are chosen arbitrarily, this is because of the fact that only stability analysis was the main concern in this work and it only needs any value of cut-off frequency for the filter. Bode plots of different transfer functions are presented in this section including the loop gains for both the cases discussed earlier. To verify the responses of different transfer functions of the system a block of frequency response analyser is used as shown in Fig. 5.14. The specifications for the converter and filter are given in Table 5.1.

Table 5.1 *Specifications for the simulations*

U_o	6V	L_f	$22\,\mu H$	C	$20\,\mu F$	I_o	1.93A
I_{in}	0.93A	C_f	$3.5\,\mu F$	r_c	$100\,m\Omega$	U_{in}	15V
D	0.53	r_{cf}	$100\,m\Omega$	r_L	$500\,m\Omega$	U_{cf}	15.93V
f_s	400KHz	r_{Lf}	$500\,m\Omega$	r_{ds1}	$15\,\mu\Omega$	U_c	15.47V
T_s	$1/\ f_s$	L	$20\,\mu H$	r_{ds2}	$15\,\mu\Omega$	R_{s-MPP}	$10.4\,\Omega$

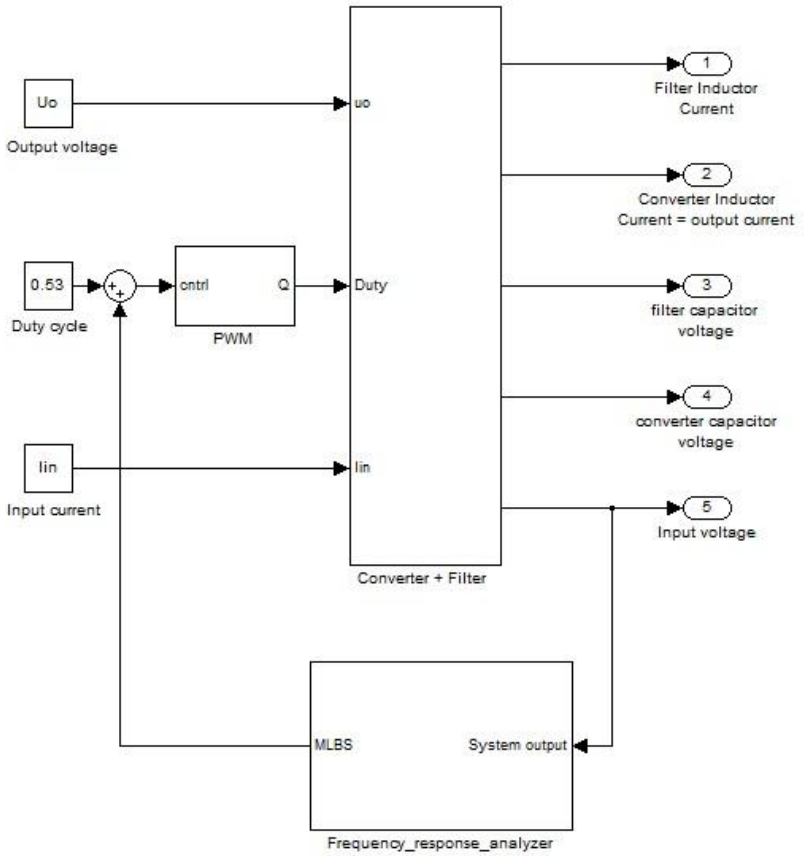

Figure 5.14 *Simulation model of the system with frequency response analyser*

There are two sets of bode plots for transfer functions as discussed in previous chapters to check the stability of different transfer functions at both the cases of control implementations. Figures 5.15, 5.16, 5.17 and 5.18 give a preview of transfer functions of converter which are affected by a source-affected (Solar panel) EMI filter, i.e. T_{oi}, G_{ci},

G_{co} and comparison of different impedances at the interface of converter and filter, respectively.

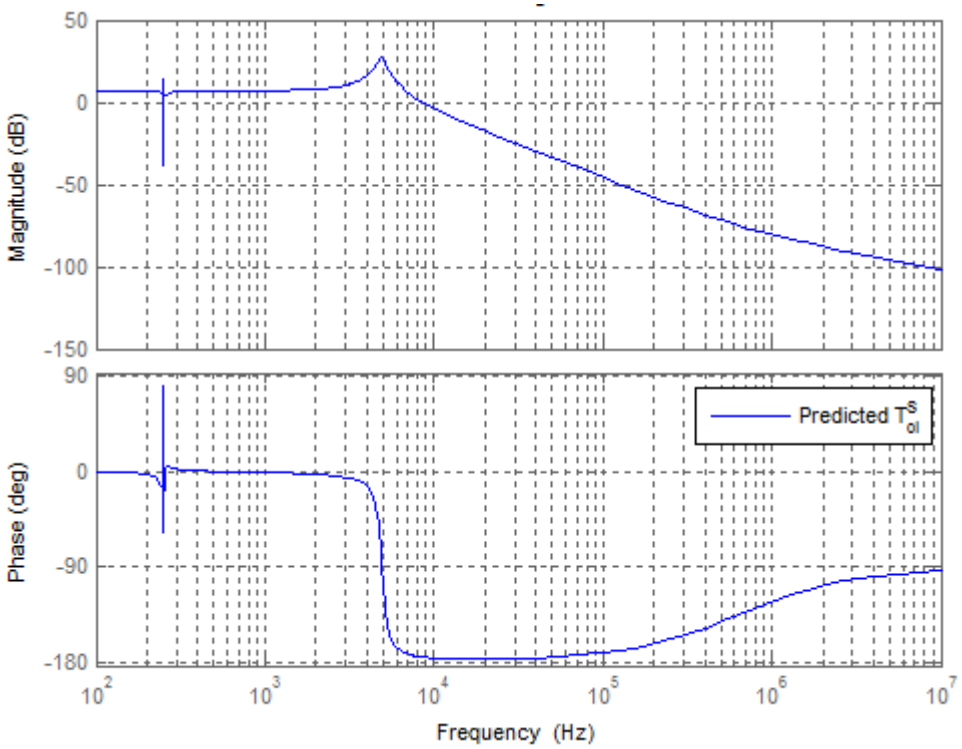

Figure 5.15 *Predicted source-affected transfer function T_{oi} of the converter*

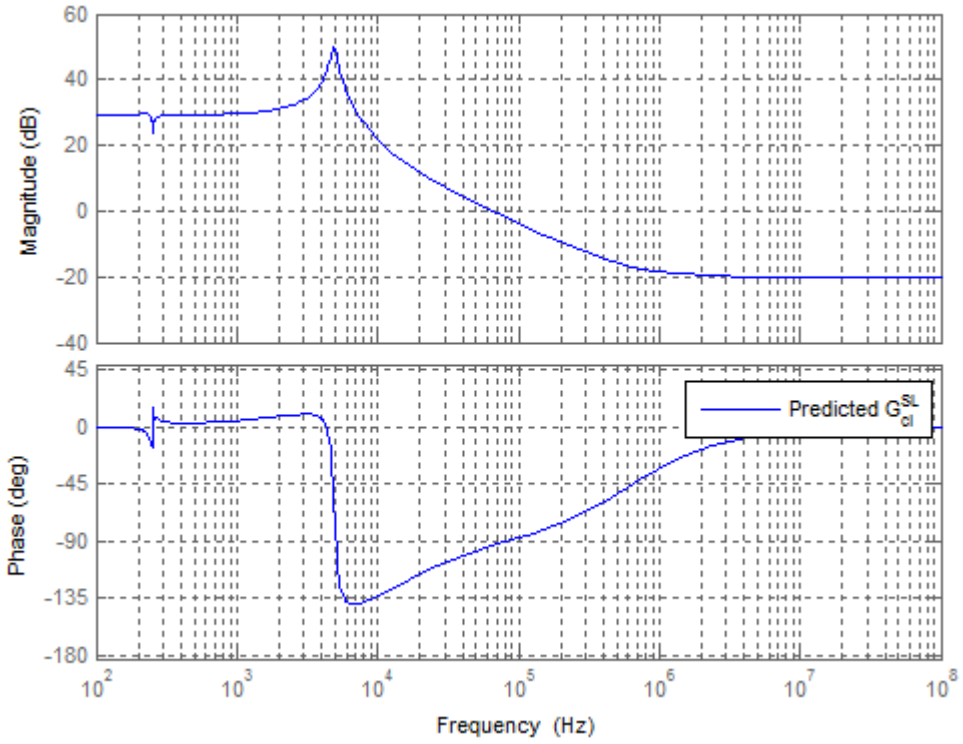

Figure 5.16 *Predicted source-affected transfer function G_{ci} of the converter*

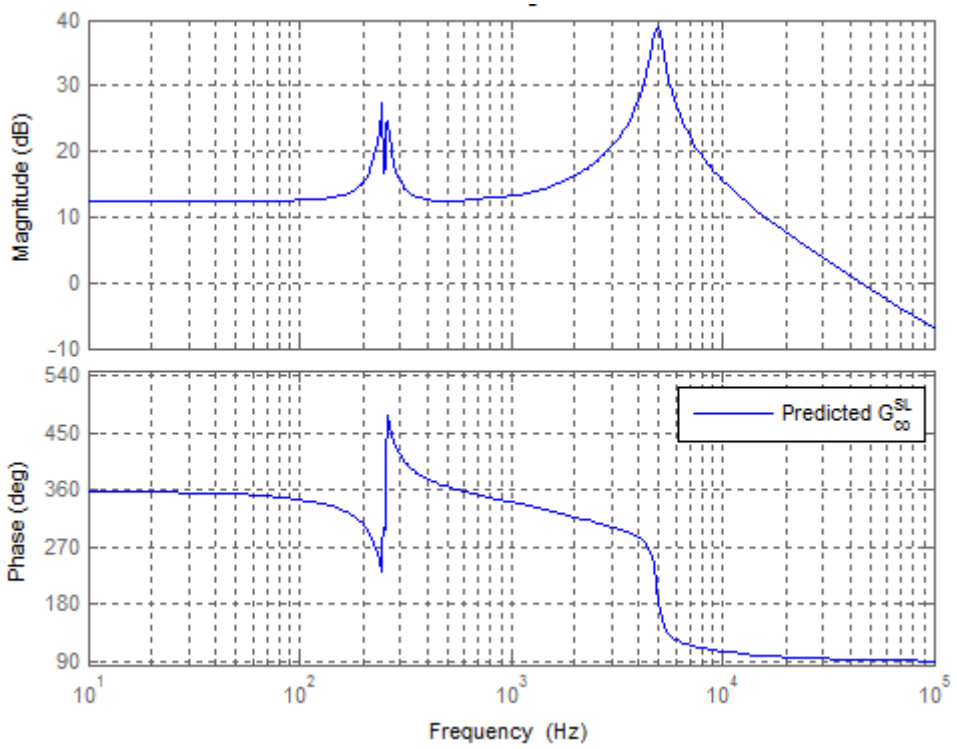

Figure 5.17 *Predicted source-affected transfer function G_{co} of the converter*

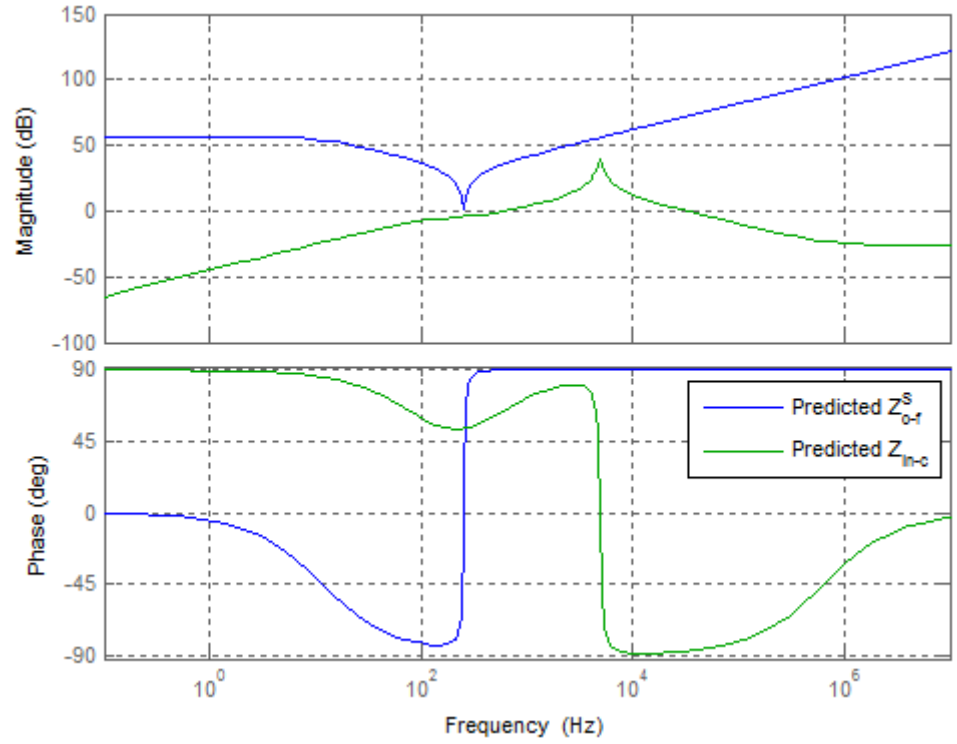

Figure 5.18 *Comparison of different impedances at the interface of converter and EMI filter*

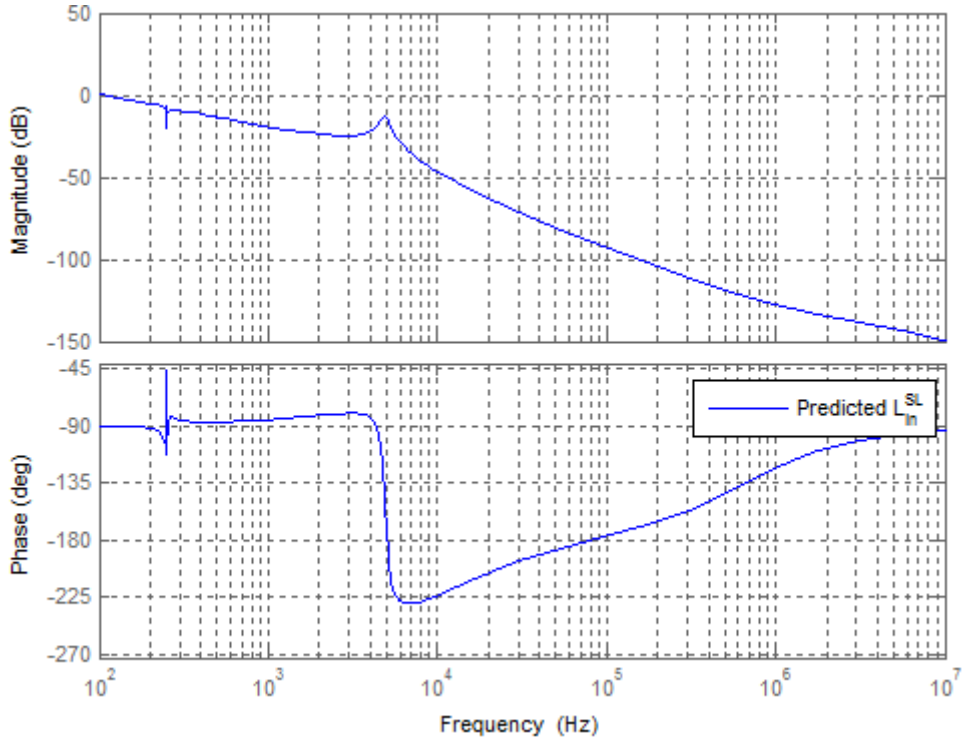

Figure 5.19 *Predicted source-affected Loop gain L_{in} of the converter when control is implemented at the interface of converter and EMI filter*

The impedances at this interface are shown in Fig. 5.18. Loop gain is shown in Fig. 5.19 which is taken when the control is implemented at the interface of converter and EMI filter, which shows that the converter works in an unstable region due to some impedance mismatching at some operating frequencies. Simulation results reveal that converter behaves differently at different regions of output power.

When the control is implemented before EMI filter, the loop gain looks stable and converter performs in a stable region, as shown in Fig. 5.20.

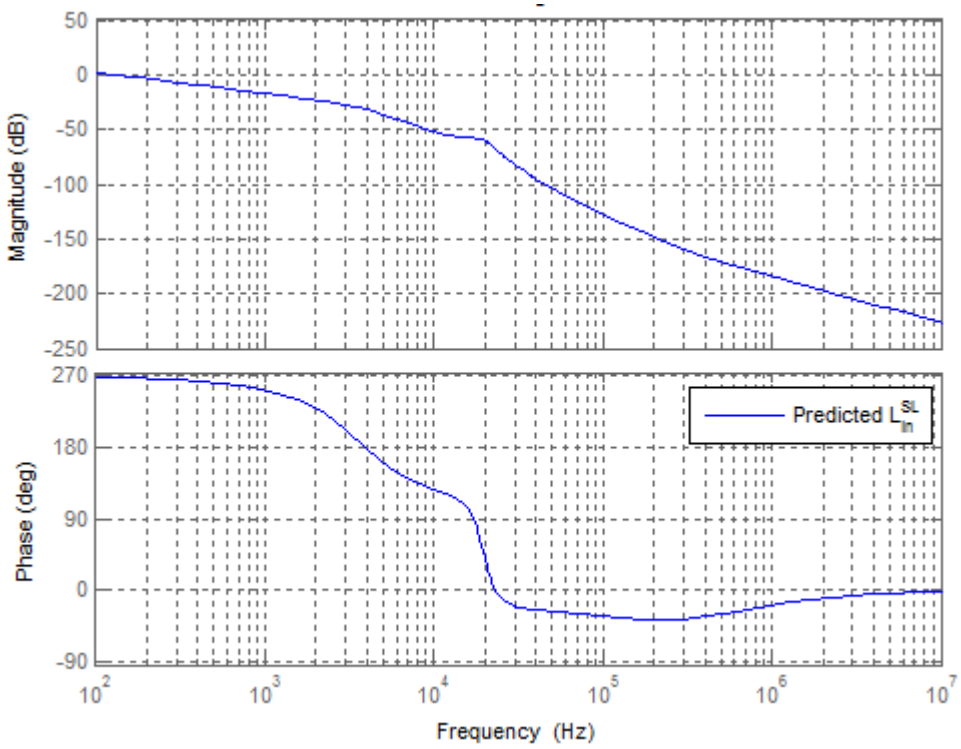

Figure 5.19 *Predicted source-affected Loop gain L_{in} of the converter when control is implemented before EMI filter*

Simulink simulations are also done for two different cases as discussed in previous chapters. The results for those simulations are given in Fig. 5.21, and 5.22. It can be clearly seen that although the ripples has been removed from the input voltage, but the operation of the converter is not stable for a long time when the control is implemented at the interface of converter and filter, which also verify the results of bode plots of loop gain transfer functions. While converter seems stable in the second case when control is implemented before EMI filter.

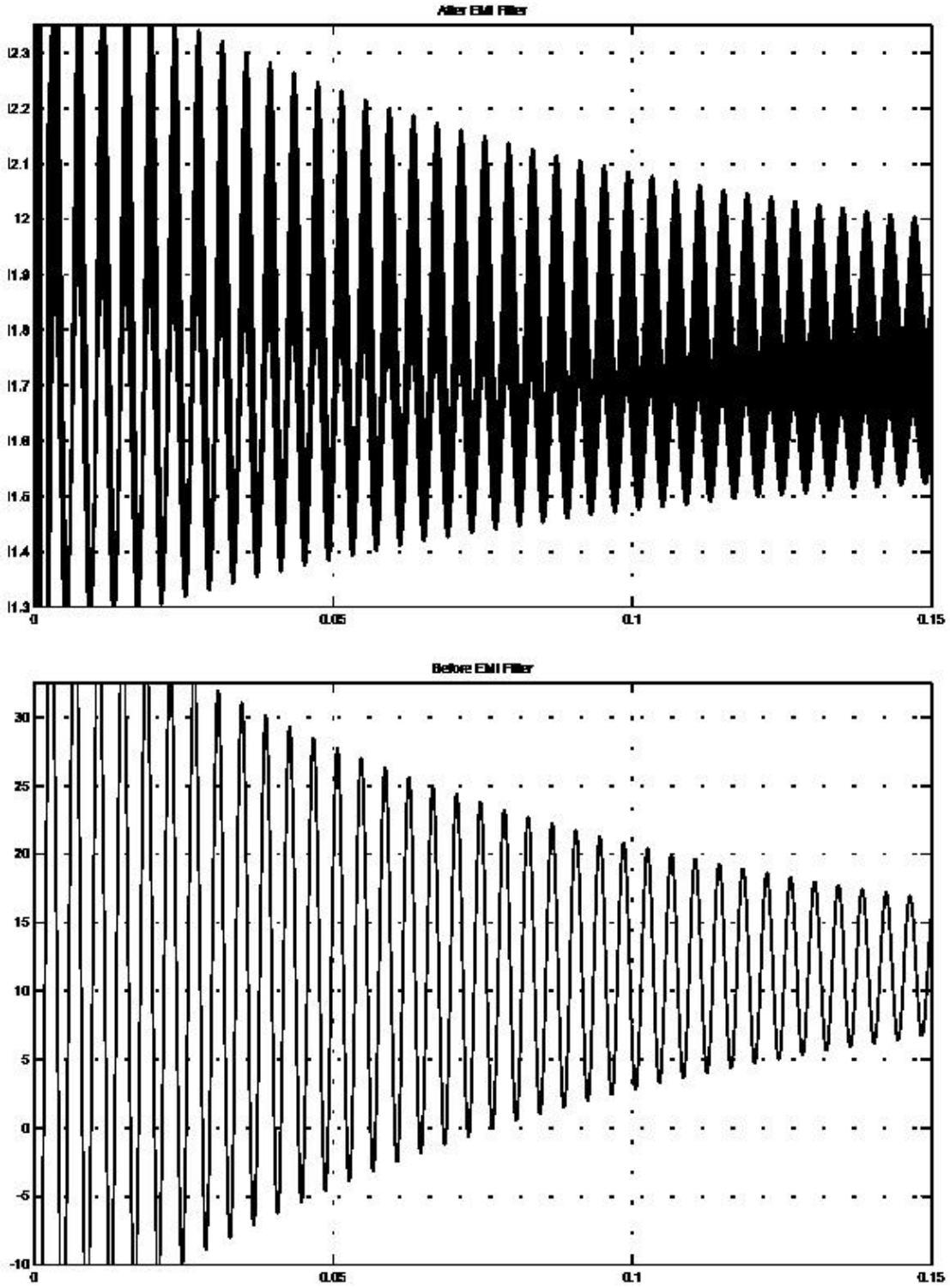

Figure 5.21 *Simulink simulation result of input voltage response of the converter when the control is implemented at the converter-filter interface*

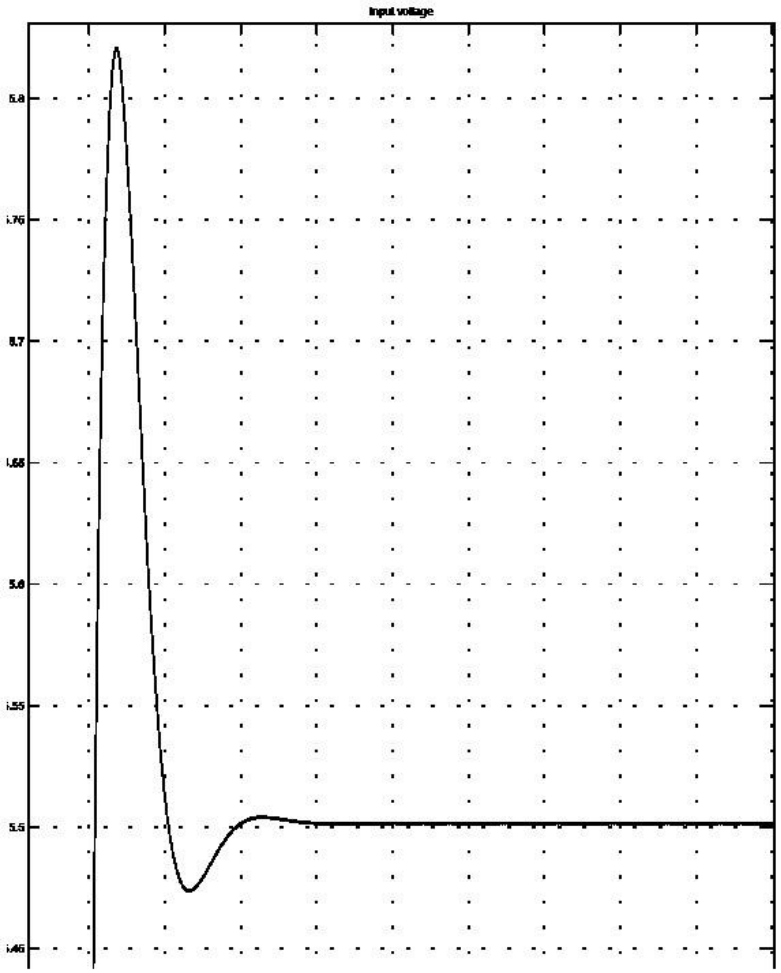

Figure 5.22 *Simulink simulation result of input voltage response of the converter when the control is implemented before EMI filter*

6 CONCLUSIONS

EMI filters have very significant role in industrial applications to prevent the surrounding atmosphere from being polluted from EMI generations of electronics circuitry. Interface of EMI filters with the power converters always need special considerations to avoid the unstable operation of power converters. In photovoltaic applications, current-sourced converters are used to achieve greater efficiency of the output power from the solar cells. When talking about current-sourced converters, which take control from the input voltage instead of output, the design of input EMI filter become a challenge to meet all the necessary specifications within a stable region.

The main objective of the work was to propose a method of implementing the input control for current-sourced converters, when an input EMI filter is needed to install at the input of the converter in solar applications, in such a way that stability of the converter is not affected. The main difficulties encountered during this thesis work were the lack of available literature related to the topic of input EMI filters for current-fed converters involved in PV applications.

The EMI filter and current-sourced converter are modelled and analysed by using the state-space averaging technique. The simulations are done using Simulink Matlab, which verify the validity of the approach of implementing the control for current-sourced converters interfaced with input EMI filters. The solar cell has its own source impedance which varies at different operating points. This source impedance should also be considered while designing the input EMI filters.

EMC standards for such type of EMI filters for PV applications are not available in the industry which is the topic of further research in this domain.

REFERENCES

[1] European Commission. Towards a 'Post-carbon society'. European research on economic incentives and social behaviour. Conference proceedings, Brussels, 24 October 2007, 50 pp.

[2] Suntio T., Maximum power point tracking methods, Lecture 9, New Applications in Electrical Energy Engineering, April 2011

[3] Leppaaho, J., Nousiainen, L., J., Puukko, J., Huusari J., Suntio T., Implementing currentfed converters by adding an input capacitor at the input of voltage-fed converter for interfacing solar generator, EPE-PEMC 2010, Ohrid, Macedonia, 2010, pp. T12-81 - T12-88.

[4] World Wide Fund Germany. Solar energy: Immense potential (WWW). Factsheet, Berlin 24 May 2004, (downloaded 4.9.2008), http://www.panda.org/about_wwf/what_we_do/climate_change/publications/fact_sheets/index.cfm?uNewsID=13444

[5] Markvart, T. Solar Electricity. 2nd edition.1994, 2000, John Wiley & Sons ltd. 280 pp.

[6] Suntio T., EMC basics, Lectures 1-4, Switched-mode converters EMC, April 2011

[7] Middlebrook, R. D, ´Cuk, S. A general unified approach to modeling switching-converter power stages. Int. Journal of Electronics, volume 42, no. 6, 1977, pp. 521-550.

[8] Sera, D., Teodorescu, R., Rodrigues, P. PV panel model based on datasheet values. IEEE International Symposium on Industrial Electronics on Industrial Electronics, ISIE 2007, June 2007, pp. 2392-2396.

[9] Esram, T., Chapman, P. L. Comparison of photovoltaic array maximum power point tracking techniques. IEEE Trans. on Energy Conversion, vol. 22, issue 2, June 2007, pp. 439-339.

[10] Shao, R., Chang, L. A new maximum power point tracking method for photovoltaic arrays using golden section search algorithm. Canadian Conference on Electrical and Computer Engineering, 4-7 May 2008, pp. 000619-000622.

[11] Rai, S.C., Kumar, U. R. Y., Naik, R. L. A novel technique for photovoltaic maximum power point tracking system. European Conference on Power Electronics and Applications, 11-14 Sept. 2005, 8 pp.

[12] Weidong, X., Ozog, N., Dunford, W. G. Topology study of photovoltaic interface for maximum power point tracking. IEEE Trans. on Industrial Electronics, vol. 54, issue 3, June 2007, pp. 1696-1704.

[13] Roinila, T., Hankaniemi, M., Suntio, T., Sippola, M., Vilkko, M. Dynamical profile of a switched-mode converter – Reality or imagination. Proc. IEEE INTELEC'07, 2007, pp. 420-427.

[14] M.C. Di Piazza, C. Serporta, G. Tine, G. Vitale, "Electromagnetic compatibility characterization of the DC side in a low power photovoltaic plant", IEEE ICIT '04, IEEE International Conference on Industrial Technology, 2004. Volume 2, 8-10 Dec. 2004 Page(s):672-677 Vol. 2

[15] Leppaaho J., "Analysis and design of Current-sourced Superbuck converter", Master of Science Thesis, Tampere University of Technology, August 2008

[16] Suntio, T., Hankaniemi, M., Karppanen, M. Analysing the dynamics of regulated converters. IEE Proc. Electric Power Applications, vol. 153, no.6, November 2006, pp. 905-910.

[17] Suntio T., Converter dynamics, Lectures 1-4, Switched-mode converter dynamics, February 2011

[18] Quin Jiang, J. Brown "Comparison of Electiomagnetic Compatibility of Different PV Inverter" Power Electronics and Drive Systems, 2001. Proceedings., 2001 4th IEEE International Conference on, Volume:l,22-25 Oct. 200 1 Pages:420 - 424 vol. 1

[19] Hankaniemi, M., Suntio, T. Dynamical modeling and control of current-output converters. International Review of Electrical Engineering, vol. 4, no. 5, September-October 2007, pp. 671-680.

[20] Huang, Y., Tse, C. K. Circuit theoretic classification of parallel connected DC-DC Converter. IEEE Trans. on Circuits and Systems, vol. 54, issue 5, May 2007, pp. 1099-1108.

[21] Deisch C. W. Simple switching control method changes converter to a current source. In IEEE PESC'78, 1978, pp. 300-306.

[22] Suntio, T., Karppanen, M., Sippola, M. Methods to characterize open-loop dynamics of current-mode-controlled converters. IEEE PESC'08, June 2008, pp. 636-642.

[23] Xiao, W., Dunford, W. G., Palmer, P.R., Capel, A. Regulation of photovoltaic voltage. IEEE Trans. on Industrial Electronics, vol. 54, issue 3, June 2007, p. 1365-1374.

[24] Liu, S., Dougal, R. A. Dynamic multiphysics model for solar array. IEEE Trans. on Energy Conversion, vol. 17, issue 2, June 2002, pp. 285 – 294.

[25] Weaver, W. W., Krein, P. T. Analysis and application of a current-sourced buck converter. In Proc. IEEE APEC'07, 2007, pp. 1664-1670.

[26] Ćuk, S. General topological properties of switching structures. in IEEE PESC'79, 1979, pp. 109-130.

[27] Tse, C. K., Lai, Y. M., Xie, R. J., Chow, M. H. L. Application of duality principle to synthesis of single-stage power-factor-correction voltage regulators. International Journal of Circuit Theory and Applications, February 2003, pp. 555-570.

[28] Leppäaho, J., Karppanen, M., Suntio T. Current-sourced buck converter. Nordic Workshop on Power and Industrial Electronics, NORPIE/2008, June 9-11, 2008, Espoo, Finland, 7 p.

[29] Desoer, C. A., Kuh, E. S. Basic circuit theory. 1969, McGraw-Hill, 876 pp.

[30] Rabinovici, R., Kaplan, B. Z. Novel DC-DC convertor schemes obtained through duality principle and topological considerations. IEE Electronic Letters, vol. 27, issue 21, 10 October 1991, pp. 1948-1950.

[31] Karppanen, M., Arminen, J., Suntio, T., Savela, K., Simola, J. Dynamical modeling and characterization of peak-current-controlled superbuck converter. IEEE Trans. on Power Electronics, vol. 23, issue 3, May 2008, pp. 1370-1380.

[32] Krein, P.T. Elements of Power Electronics. New York, 1998, Oxford University Press.

[33] Suntio, T. Unified average and small-signal modeling of direct-on-time-control. IEEE Trans. on Industrial Electronics, vol. 53, no. 1, February 2006, pp. 287-295.

[34] Tse, C. K. Linear circuit analysis. Addison Wesley Longman, Harlow Ltd., England 1998, 307 pp.

APPENDIX 1: Matlab File For Solving H-parameters for Case I

```
%#########################################################################
%#########################################################################
%%%%% Current-fed Converter and EMI-filter design ##################
%#########################################################################
%#########################################################################

clear all

%%%%% Source impedance or admittance (of solar module)
Zs = 700;  % low-freq. impedance (resistance) of solar module
Ys = 1/Zs;  % same as an admittance

%%%%% Model for CF-filter

L_f = 20e-3;
C_f = 20e-6;
rc_f = 10e-3;
rL_f = 10e-3;

s = tf('s')
% Symbolic transfer functions created in file filter_symbolic.m
Zin_f = ((C_f*L_f*rc_f)*s^2 + (L_f + C_f*rL_f*rc_f)*s +
rL_f)/((C_f*L_f)*s^2 + (C_f*rL_f + C_f*rc_f)*s + 1);
Gio_f = ((C_f*rc_f)*s + 1)/((C_f*L_f)*s^2 + (C_f*rL_f + C_f*rc_f)*s +
1);
Toi_f = ((C_f*rc_f)*s + 1)/((C_f*L_f)*s^2 + (C_f*rL_f + C_f*rc_f)*s +
1);
Yo_f = -((-C_f)*s)/((C_f*L_f)*s^2 + (C_f*rL_f + C_f*rc_f)*s + 1);

% Source effects for the filter:
Zin_f_oco = Zin_f + Gio_f*Toi_f/Yo_f; % Zin in at open-circuited input
(special transfer function)
 Zin_f_S = Zin_f/(1 + Zin_f*Ys);
Toi_f_S = Toi_f/(1 + Zin_f*Ys);
Gio_f_S = Gio_f/(1 + Zin_f*Ys);
Yo_f_S = (1 + Ys*Zin_f_oco)*Yo_f/(1 + Zin_f*Ys);

% Bode diagrams for the filter transfer functions:

%%%%% Model for CF boost converter
Uo = 6;
Iin = 0.93;
Du = 0.53;
IL = Iin/(1-Du);
fs = 400000;
Ts = 1/fs;
Io = IL;
rc = 0.05;
ri = 0.1;
rds = 0.015;
rd = 0.015;     % synchronous mode rd = rds
Ud = 0.0;       % synchronous mode Ud = 0

Uc = (((1-Du)*rds + Du*rd + (1-Du)*rc + ri)*IL - (1-Du)*rc*Iin +
Du*Ud+Uo)/(1-Du);
```

```
L1 = 47e-6;
C1 = 5e-6;

% Symbolic transfer functions created in file converter_symbolic.m
Zin = ((-C1*L1*rc)*s^2 + (C1*Du^2*rc^2 - L1 - C1*rc*rds - C1*rc*ri -
C1*Du*rc^2 - C1*Du*rc*rd + C1*Du*rc*rds)*s + Du*rds - ri - Du*rc -
Du*rd - rds + Du^2*rc)/((-C1*L1)*s^2 + (C1*Du*rc - C1*rds - C1*ri -
C1*rc - C1*Du*rd + C1*Du*rds)*s - Du^2 + 2*Du - 1) ;
Gio = ((C1*Du*rc - C1*rc)*s + Du - 1)/((-C1*L1)*s^2 + (C1*Du*rc -
C1*rds - C1*ri - C1*rc - C1*Du*rd + C1*Du*rds)*s - Du^2 + 2*Du - 1);
Toi = ((C1*Du*rc - C1*rc)*s + Du - 1)/((-C1*L1)*s^2 + (C1*Du*rc -
C1*rds - C1*ri - C1*rc - C1*Du*rd + C1*Du*rds)*s - Du^2 + 2*Du - 1);
Yo = -(C1*s)/((-C1*L1)*s^2 + (C1*Du*rc - C1*rds - C1*ri - C1*rc -
C1*Du*rd + C1*Du*rds)*s - Du^2 + 2*Du - 1);
Gci = ((C1*IL*L1*rc)*s^2 + (IL*L1 + C1*Uc*rc + C1*Ud*rc + C1*IL*rc^2 -
2*C1*Du*IL*rc^2 + C1*Du^2*IL*rc^2 - C1*Du*Uc*rc - C1*Du*Ud*rc +
C1*IL*rc*rd + C1*IL*rc*ri)*s + Uc + Ud + IL*rc + IL*rd + IL*ri - Du*Uc
- Du*Ud - 2*Du*IL*rc + Du^2*IL*rc)/((C1*L1)*s^2 + (C1*rc + C1*rds +
C1*ri - C1*Du*rc + C1*Du*rd - C1*Du*rds)*s + Du^2 - 2*Du + 1);
Gco = ((C1*IL*rds - C1*Ud - C1*IL*rd - C1*Uc + C1*Du*IL*rc)*s + IL -
Du*IL)/((C1*L1)*s^2 + (C1*rc + C1*rds + C1*ri - C1*Du*rc + C1*Du*rd -
C1*Du*rds)*s + Du^2 - 2*Du + 1);


M_Ys = Yo_f_S; % Source admittance seen by the converter: Filter out-
put admittance with effect of solar module
M_ZL = 0.01 ;% Load impedance seen by the converter (assumed e.g. bat-
tery with low resistance)

% special transfer functions:
Zin_oc = Zin + ((Gio*Toi)/Yo);   % Open-circuit input impedance
Zin_inf = Zin - ((Gio*Gci)/Gco); % ideal input impedance

% Some of the source-affected and load-affected transfer functions:
P_Gio_L = Gio/(1 + Yo*M_ZL);                    % Predicted load-
affected Gio
P_Zin_L = Zin + (M_ZL*Toi*Gio)/(1 + Yo*M_ZL);   % Predicted load-
affected Zin
P_Toi_S = Toi/(1 + (M_Ys*Zin));                 % Predicted source-
affected Toi
P_Yo_S = Yo*((1 + M_Ys*Zin_oc)/(1 + M_Ys*Zin)); % Predicted source-
affected Yo

P_Gco_L = Gco/(1 + Yo*M_ZL);                    % Predicted load-
affected Gco
P_Gco_SL = P_Gco_L*((1 + M_Ys*Zin_inf)/(1 + M_Ys*P_Zin_L)) % Predicted
source and load-affected Gco

P_Gci_L = Gci + (M_ZL*Toi*Gco)/(1 + Yo*M_ZL);   % Predicted load-
affected Gci
P_Gci_SL = P_Gci_L/(1 + (M_Ys*P_Zin_L));        % Predicted source and
load-affected Gci

figure(5);
bode(P_Gio_L);
legend('Predicted G_{io-o}^L');

figure(6);
```

```
bode(P_Zin_L);
legend('Predicted Z_{in-o}^L')

figure(7);
bode(P_Toi_S);
legend('Predicted T_{oi-o}^S');

figure(8);
bode(P_Yo_S);
legend('Predicted Y_{o-o}^S');

figure(9);
bode(P_Gci_SL);
legend('Predicted G_{ci-o}^S^L');

figure(10);
bode(P_Gco_SL);
legend('Predicted G_{co-o}^S^L');


%%% Controller design and loop gain

% modulator gain:
Ga = 1/2;

% input voltage scaling:
Hv = 0.45;

% I-controller (component values can be changed to have desired loop
gain):
C_ctrl = 100e-9;
R_ctrl = 100000;

Gcc = 1/(s*C_ctrl*R_ctrl)

% nominal input-voltage loop gain:
Lin = Gcc*Ga*Hv*Gci

% nominal closed-loop input impedance:
Zin_c = Zin/(1 + Lin)

% Input-voltage loop gain with source and load effects:
Lin_SL = Gcc*Ga*Hv*P_Gci_SL;

%%%% Comparison of source-affected output impedance (filter) and dif-
ferent input impedances (converter):
figure(11)
bode(1/Yo_f_S, P_Zin_L, Zin_c, Zin_oc, Zin_inf);
legend('Predicted Z_{o-f}^S','Predicted Z_{in-o}^L','Predicted Z_{in-
oc}', 'Predicted Z_{in-inf}', 'Predicted Z_{in-c}' );

%%%% Input-voltage loop gain with the source interactions (i.e. solar
panel and filter) and load effects (battery impedance)
figure(12);
bode(Lin_SL);
legend('Predicted L_{in}^S^L');
```

APPENDIX 2: Matlab File For Solving H-parameters for case II

```
%#########################################################################
%#########################################################################
%%%%% Current-fed Converter and EMI-filter design ##################
%#########################################################################
%#########################################################################

clear all

%%%%% Source impedance or admittance (of solar module)
Zs = 789;  % low-freq. impedance (resistance) of solar module
Ys = 1/Zs;  % same as an admittance

%%%%% Model for CF with input filter as power stage boost converter

Uo = 6;
Iin = 0.93;
Du = 0.53;
Du2 = 1-Du;
fs = 400000;
Ts = 1/fs;

L1 = 22e-6;
C1 = 3.5e-6;
rc1 = 100e-3;
rL1 = 500e-3;

L2 = 20e-6;
C2 = 20e-6;
rc2 = 100e-3;
rL2 = 500e-3;

rds1 = 0.015;
rds2 = 0.015;

IL1 = Iin;
IL2 = Iin/Du2;

Uc1 = Uo/Du2 + ((rL1+rc2)*Du2^2 + Du*rds1 + Du*rc2 + Du2*rds2 +
rL2)/(Du2^2)
Uc2 = Uc1 - rL1*Iin

s = tf('s');

% Symbolic transfer functions created in file sy-
molic_CFBOOST_filter_included.m
Zin = ((C1*C2*L1*L2^2*rc1)*s^4 + (C2*L1*L2^2 - C1*C2*L2^2*rc1^2 +
C1*C2*L1*L2*rc1^2 + C1*C2*L1*L2*rL1*rc1 + C1*C2*L1*L2*rL2*rc1 +
C1*C2*L1*L2*rc1*rc2 + C1*C2*Du2*L1*L2*rc1*rc2 +
C1*C2*Du*L1*L2*rc1*rds1 + C1*C2*Du2*L1*L2*rc1*rds2)*s^3 + (C1*L2^2*rc1
- C2*L2^2*rc1 + C2*L1*L2*rL1 + C2*L1*L2*rL2 + C2*L1*L2*rc1 +
C2*L1*L2*rc2 + C1*C2*L1*rL2*rc1^2 - C1*C2*L2*rL2*rc1^2 +
C2*Du2*L1*L2*rc2 + C2*Du*L1*L2*rds1 + C2*Du2*L1*L2*rds2 -
C1*C2*Du2^2*L2*rc1*rc2^2 + C1*Du*Du2*L1*L2*rc1 + C1*C2*L1*rL1*rL2*rc1
+ C1*C2*L1*rL2*rc1*rc2 + C1*C2*Du2*L1*rc1*rc2^2 +
C1*C2*Du2*L1*rc1^2*rc2 - C1*C2*Du2*L2*rc1^2*rc2 +
```

```
C1*C2*Du*L1*rc1^2*rds1 + C1*C2*Du2*L1*rc1^2*rds2 -
C1*C2*Du*L2*rc1^2*rds1 - C1*C2*Du2*L2*rc1^2*rds2 +
C1*C2*Du2*L1*rL1*rc1*rc2 + C1*C2*Du*L1*rL1*rc1*rds1 +
C1*C2*Du2*L1*rL1*rc1*rds2 + C1*C2*Du*L1*rc1*rc2*rds1 +
C1*C2*Du2*L1*rc1*rc2*rds2)*s^2 + (L2^2 + C2*Du2*L1*rc2^2 -
C2*Du2^2*L2*rc2^2 + Du*Du2*L1*L2 + C2*L1*rL1*rL2 + C1*L2*rL2*rc1 +
C2*L1*rL2*rc1 + C2*L1*rL2*rc2 - C2*L2*rL2*rc1 + C2*Du2*L1*rL1*rc2 +
C2*Du*L1*rL1*rds1 + C2*Du2*L1*rL1*rds2 + C1*Du2*L2*rc1*rc2 +
C2*Du2*L1*rc1*rc2 - C2*Du2*L2*rc1*rc2 + C1*Du*L2*rc1*rds1 +
C2*Du*L1*rc1*rds1 + C2*Du*L1*rc2*rds1 + C1*Du2*L2*rc1*rds2 +
C2*Du2*L1*rc1*rds2 + C2*Du2*L1*rc2*rds2 - C2*Du*L2*rc1*rds1 -
C2*Du2*L2*rc1*rds2 + C1*Du*Du2*L1*rc1^2 - C1*Du*Du2*L2*rc1^2 -
C1*Du2^2*L2*rc1*rc2 + C1*Du*Du2*L1*rL1*rc1 + C1*Du*Du2*L1*rc1*rc2 -
C1*Du*Du2*L2*rc1*rc2)*s + L2*rL2 + Du2*L2*rc2 + Du*L2*rds1 +
Du2*L2*rds2 - Du2^2*L2*rc2 + Du*Du2*L1*rL1 + Du*Du2*L1*rc1 +
Du*Du2*L1*rc2 - Du*Du2*L2*rc1 - Du*Du2*L2*rc2)/((C1*C2*L1*L2^2)*s^4 +
(C1*C2*L1*L2*rL1 + C1*C2*L1*L2*rL2 + C1*C2*L1*L2*rc1 + C1*C2*L1*L2*rc2
+ C1*C2*Du2*L1*L2*rc2 + C1*C2*Du*L1*L2*rds1 +
C1*C2*Du2*L1*L2*rds2)*s^3 + (C1*L2^2 + C2*L2^2 + C1*C2*L1*rL1*rL2 +
C1*C2*L1*rL2*rc1 + C1*C2*L1*rL2*rc2 + C1*C2*Du2*L1*rc2^2 -
C1*C2*Du2^2*L2*rc2^2 + C1*Du*Du2*L1*L2 + C1*C2*Du2*L1*rL1*rc2 +
C1*C2*Du*L1*rL1*rds1 + C1*C2*Du2*L1*rL1*rds2 + C1*C2*Du2*L1*rc1*rc2 +
C1*C2*Du*L1*rc1*rds1 + C1*C2*Du*L1*rc2*rds1 + C1*C2*Du2*L1*rc1*rds2 +
C1*C2*Du2*L1*rc2*rds2)*s^2 + (C1*L2*rL2 + C2*L2*rL2 - C1*Du2^2*L2*rc2
+ C1*Du2*L2*rc2 + C2*Du2*L2*rc2 + C1*Du*L2*rds1 + C1*Du2*L2*rds2 +
C2*Du*L2*rds1 + C2*Du2*L2*rds2 + C1*Du*Du2*L1*rL1 + C1*Du*Du2*L1*rc1 +
C1*Du*Du2*L1*rc2 - C1*Du*Du2*L2*rc2)*s + Du*Du2*L2)
Gio = ((C1*C2*Du2*L2*rc1*rc2)*s^2 + (C1*Du2*L2*rc1 + C2*Du2*L2*rc2)*s
+ Du2*L2)/((C1*C2*L1*L2^2)*s^4 + (C1*C2*L1*L2*rL1 + C1*C2*L1*L2*rL2 +
C1*C2*L1*L2*rc1 + C1*C2*L1*L2*rc2 + C1*C2*Du2*L1*L2*rc2 +
C1*C2*Du*L1*L2*rds1 + C1*C2*Du2*L1*L2*rds2)*s^3 + (C1*L2^2 + C2*L2^2 +
C1*C2*L1*rL1*rL2 + C1*C2*L1*rL2*rc1 + C1*C2*L1*rL2*rc2 +
C1*C2*Du2*L1*rc2^2 - C1*C2*Du2^2*L2*rc2^2 + C1*Du*Du2*L1*L2 +
C1*C2*Du2*L1*rL1*rc2 + C1*C2*Du*L1*rL1*rds1 + C1*C2*Du2*L1*rL1*rds2 +
C1*C2*Du2*L1*rc1*rc2 + C1*C2*Du*L1*rc1*rds1 + C1*C2*Du*L1*rc2*rds1 +
C1*C2*Du2*L1*rc1*rds2 + C1*C2*Du2*L1*rc2*rds2)*s^2 + (C1*L2*rL2 +
C2*L2*rL2 - C1*Du2^2*L2*rc2 + C1*Du2*L2*rc2 + C2*Du2*L2*rc2 +
C1*Du*L2*rds1 + C1*Du2*L2*rds2 + C2*Du*L2*rds1 + C2*Du2*L2*rds2 +
C1*Du*Du2*L1*rL1 + C1*Du*Du2*L1*rc1 + C1*Du*Du2*L1*rc2 -
C1*Du*Du2*L2*rc2)*s + Du*Du2*L2)
Toi = ((C1*C2*Du2*L2*rc1*rc2)*s^2 + (C1*Du*L2*rc1 + C2*Du2*L2*rc2)*s +
Du*L2)/((C1*C2*L1*L2^2)*s^4 + (C1*C2*L1*L2*rL1 + C1*C2*L1*L2*rL2 +
C1*C2*L1*L2*rc1 + C1*C2*L1*L2*rc2 + C1*C2*Du2*L1*L2*rc2 +
C1*C2*Du*L1*L2*rds1 + C1*C2*Du2*L1*L2*rds2)*s^3 + (C1*L2^2 + C2*L2^2 +
C1*C2*L1*rL1*rL2 + C1*C2*L1*rL2*rc1 + C1*C2*L1*rL2*rc2 +
C1*C2*Du2*L1*rc2^2 - C1*C2*Du2^2*L2*rc2^2 + C1*Du*Du2*L1*L2 +
C1*C2*Du2*L1*rL1*rc2 + C1*C2*Du*L1*rL1*rds1 + C1*C2*Du2*L1*rL1*rds2 +
C1*C2*Du2*L1*rc1*rc2 + C1*C2*Du*L1*rc1*rds1 + C1*C2*Du*L1*rc2*rds1 +
C1*C2*Du2*L1*rc1*rds2 + C1*C2*Du2*L1*rc2*rds2)*s^2 + (C1*L2*rL2 +
C2*L2*rL2 - C1*Du2^2*L2*rc2 + C1*Du2*L2*rc2 + C2*Du2*L2*rc2 +
C1*Du*L2*rds1 + C1*Du2*L2*rds2 + C2*Du*L2*rds1 + C2*Du2*L2*rds2 +
C1*Du*Du2*L1*rL1 + C1*Du*Du2*L1*rc1 + C1*Du*Du2*L1*rc2 -
C1*Du*Du2*L2*rc2)*s + Du*Du2*L2)
Yo = -((-C1*C2*L1*L2)*s^3 + (- C1*C2*L1*rL1 - C1*C2*L1*rc1 -
C1*C2*L1*rc2)*s^2 + (- C1*L2 - C2*L2)*s)/((C1*C2*L1*L2^2)*s^4 +
(C1*C2*L1*L2*rL1 + C1*C2*L1*L2*rL2 + C1*C2*L1*L2*rc1 + C1*C2*L1*L2*rc2
+ C1*C2*Du2*L1*L2*rc2 + C1*C2*Du*L1*L2*rds1 +
C1*C2*Du2*L1*L2*rds2)*s^3 + (C1*L2^2 + C2*L2^2 + C1*C2*L1*rL1*rL2 +
C1*C2*L1*rL2*rc1 + C1*C2*L1*rL2*rc2 + C1*C2*Du2*L1*rc2^2 -
C1*C2*Du2^2*L2*rc2^2 + C1*Du*Du2*L1*L2 + C1*C2*Du2*L1*rL1*rc2 +
C1*C2*Du*L1*rL1*rds1 + C1*C2*Du2*L1*rL1*rds2 + C1*C2*Du2*L1*rc1*rc2 +
```

```
C1*C2*Du*L1*rc1*rds1 + C1*C2*Du*L1*rc2*rds1 + C1*C2*Du2*L1*rc1*rds2 +
C1*C2*Du2*L1*rc2*rds2)*s^2 + (C1*L2*rL2 + C2*L2*rL2 - C1*Du2^2*L2*rc2
+ C1*Du2*L2*rc2 + C2*Du2*L2*rc2 + C1*Du*L2*rds1 + C1*Du2*L2*rds2 +
C2*Du*L2*rds1 + C2*Du2*L2*rds2 + C1*Du*Du2*L1*rL1 + C1*Du*Du2*L1*rc1 +
C1*Du*Du2*L1*rc2 - C1*Du*Du2*L2*rc2)*s + Du*Du2*L2)
Gci = ((-C1*C2*IL2*L2^2*rc1*rc2)*s^3 + (C1*IL2*L2^2*rc1 -
C2*IL2*L2^2*rc2 + C1*C2*Du2*IL1*L2*rc1*rc2^2 -
2*C1*C2*Du2*IL2*L2*rc1*rc2^2 + C1*C2*Du2*L2*Uc2*rc1*rc2 -
C1*C2*IL2*L2*rL2*rc1*rc2 - C1*C2*Du*IL2*L2*rc1*rc2*rds1 +
C1*C2*Du2*IL2*L2*rc1*rc2*rds1 - 2*C1*C2*Du2*IL2*L2*rc1*rc2*rds2)*s^2 +
(IL2*L2^2 + C1*IL2*L2*rL2*rc1 - C2*IL2*L2*rL2*rc2 +
C2*Du2*IL1*L2*rc2^2 - 2*C2*Du2*IL2*L2*rc2^2 + C1*Du*L2*Uc2*rc1 +
C2*Du2*L2*Uc2*rc2 + C1*Du*IL1*L2*rc1*rc2 - C1*Du*IL2*L2*rc1*rc2 +
C1*Du2*IL2*L2*rc1*rc2 + 2*C1*Du*IL2*L2*rc1*rds1 -
C1*Du*IL2*L2*rc1*rds2 + C1*Du2*IL2*L2*rc1*rds2 - C2*Du*IL2*L2*rc2*rds1
+ C2*Du2*IL2*L2*rc2*rds1 - 2*C2*Du2*IL2*L2*rc2*rds2 -
C1*Du2^2*IL2*L2*rc1*rc2 - C1*Du*Du2*IL2*L2*rc1*rc2)*s + Du*L2*Uc2 +
IL2*L2*rL2 - Du2^2*IL2*L2*rc2 + Du*IL1*L2*rc2 - Du*IL2*L2*rc2 +
Du2*IL2*L2*rc2 + 2*Du*IL2*L2*rds1 - Du*IL2*L2*rds2 + Du2*IL2*L2*rds2 -
Du*Du2*IL2*L2*rc2)/((C1*C2*L1*L2^2)*s^4 + (C1*C2*L1*L2*rL1 +
C1*C2*L1*L2*rL2 + C1*C2*L1*L2*rc1 + C1*C2*L1*L2*rc2 +
C1*C2*Du2*L1*L2*rc2 + C1*C2*Du*L1*L2*rds1 + C1*C2*Du2*L1*L2*rds2)*s^3
+ (C1*L2^2 + C2*L2^2 + C1*C2*L1*rL1*rL2 + C1*C2*L1*rL2*rc1 +
C1*C2*L1*rL2*rc2 + C1*C2*Du2*L1*rc2^2 - C1*C2*Du2^2*L2*rc2^2 +
C1*Du*Du2*L1*L2 + C1*C2*Du2*L1*rL1*rc2 + C1*C2*Du*L1*rL1*rds1 +
C1*C2*Du2*L1*rL1*rds2 + C1*C2*Du2*L1*rc1*rc2 + C1*C2*Du*L1*rc1*rds1 +
C1*C2*Du*L1*rc2*rds1 + C1*C2*Du2*L1*rc1*rds2 +
C1*C2*Du2*L1*rc2*rds2)*s^2 + (C1*L2*rL2 + C2*L2*rL2 - C1*Du2^2*L2*rc2
+ C1*Du2*L2*rc2 + C2*Du2*L2*rc2 + C1*Du*L2*rds1 + C1*Du2*L2*rds2 +
C2*Du*L2*rds1 + C2*Du2*L2*rds2 + C1*Du*Du2*L1*rL1 + C1*Du*Du2*L1*rc1 +
C1*Du*Du2*L1*rc2 - C1*Du*Du2*L2*rc2)*s + Du*Du2*L2)
Gco = ((C1*C2*L1*L2*Uc2 + C1*C2*IL1*L1*L2*rc2 - C1*C2*IL2*L1*L2*rc2 +
C1*C2*IL2*L1*L2*rds1 - C1*C2*IL2*L1*L2*rds2)*s^3 + (C1*C2*IL1*L1*rc2^2
- C1*C2*IL2*L1*rc2^2 - C1*Du2*IL2*L1*L2 + C1*C2*L1*Uc2*rL1 +
C1*C2*L1*Uc2*rc1 + C1*C2*L1*Uc2*rc2 + C1*C2*IL1*L1*rL1*rc2 -
C1*C2*IL2*L1*rL1*rc2 + C1*C2*IL2*L1*rL1*rds1 - C1*C2*IL2*L1*rL1*rds2 +
C1*C2*IL1*L1*rc1*rc2 - C1*C2*IL2*L1*rc1*rc2 + C1*C2*IL2*L1*rc1*rds1 -
C1*C2*IL2*L1*rc1*rds2 + C1*C2*IL2*L1*rc2*rds1 - C1*C2*IL2*L1*rc2*rds2
- C1*C2*Du2*IL2*L2*rc2^2)*s^2 + (C1*L2*Uc2 + C2*L2*Uc2 + C1*IL1*L2*rc2
- C1*IL2*L2*rc2 + C2*IL1*L2*rc2 - C2*IL2*L2*rc2 + C1*IL2*L2*rds1 -
C1*IL2*L2*rds2 + C2*IL2*L2*rds1 - C2*IL2*L2*rds2 - C1*Du2*IL2*L1*rL1 -
C1*Du2*IL2*L1*rc1 - C1*Du2*IL2*L1*rc2)*s - Du2*IL2*L2)/((-
C1*C2*L1*L2^2)*s^4 + (- C1*C2*L1*L2*rL1 - C1*C2*L1*L2*rL2 -
C1*C2*L1*L2*rc1 - C1*C2*L1*L2*rc2 - C1*C2*Du2*L1*L2*rc2 -
C1*C2*Du*L1*L2*rds1 - C1*C2*Du2*L1*L2*rds2)*s^3 +
(C1*C2*Du2^2*L2*rc2^2 - C2*L2^2 - C1*C2*L1*rL1*rL2 - C1*C2*L1*rL2*rc1
- C1*C2*L1*rL2*rc2 - C1*C2*Du2*L1*rc2^2 - C1*L2^2 - C1*Du*Du2*L1*L2 -
C1*C2*Du2*L1*rL1*rc2 - C1*C2*Du*L1*rL1*rds1 - C1*C2*Du2*L1*rL1*rds2 -
C1*C2*Du2*L1*rc1*rc2 - C1*C2*Du*L1*rc1*rds1 - C1*C2*Du*L1*rc2*rds1 -
C1*C2*Du2*L1*rc1*rds2 - C1*C2*Du2*L1*rc2*rds2)*s^2 + (C1*Du2^2*L2*rc2
- C2*L2*rL2 - C1*L2*rL2 - C1*Du2*L2*rc2 - C2*Du2*L2*rc2 -
C1*Du*L2*rds1 - C1*Du2*L2*rds2 - C2*Du*L2*rds1 - C2*Du2*L2*rds2 -
C1*Du*Du2*L1*rL1 - C1*Du*Du2*L1*rc1 - C1*Du*Du2*L1*rc2 +
C1*Du*Du2*L2*rc2)*s - Du*Du2*L2)

M_Ys = Ys % Source admittance seen by the converter
M_ZL = 0.01 % Load impedance seen by the converter (assumed e.g. bat-
tery with low resistance)

% special transfer functions:
Zin_oc = Zin + ((Gio*Toi)/Yo);   % Open-circuit input impedance
```

```
Zin_inf = Zin - ((Gio*Gci)/Gco); % ideal input impedance

% Some of the source-affected and load-affected transfer functions:
P_Gio_L = Gio/(1 + Yo*M_ZL);                    % Predicted load-
affected Gio
P_Zin_L = Zin + (M_ZL*Toi*Gio)/(1 + Yo*M_ZL);   % Predicted load-
affected Zin
P_Toi_S = Toi/(1 + (M_Ys*Zin));                 % Predicted source-
affected Toi
P_Yo_S = Yo*((1 + M_Ys*Zin_oc)/(1 + M_Ys*Zin)); % Predicted source-
affected Yo

P_Gco_L = Gco/(1 + Yo*M_ZL);                    % Predicted load-
affected Gco
P_Gco_SL = P_Gco_L*((1 + M_Ys*Zin_inf)/(1 + M_Ys*P_Zin_L)) % Predicted
source and load-affected Gco

P_Gci_L = Gci + (M_ZL*Toi*Gco)/(1 + Yo*M_ZL);   % Predicted load-
affected Gci
P_Gci_SL = P_Gci_L/(1 + (M_Ys*P_Zin_L));        % Predicted source and
load-affected Gci
% %%% Controller design and loop gain

% modulator gain:
Ga = 1/2;

% input voltage scaling:
Hv = 0.45;

% I-controller (component values can be changed to have desired loop
gain):
C_ctrl = 100e-9;
R_ctrl = 100000;

Gcc = 1/(s*C_ctrl*R_ctrl)

% nominal input-voltage loop gain:
Lin = Gcc*Ga*Hv*Gci

% nominal closed-loop input impedance:
Zin_c = Zin/(1 + Lin)

% Input-voltage loop gain with source and load effects:
Lin_SL = Gcc*Ga*Hv*P_Gci_SL;

%%%% Input-voltage loop gain with the source interactions (i.e. solar
panel
%%%% and filter) and load effects (battery impedance)
figure(22);
bode(Lin_SL);
legend('Predicted L_{in}^S^L');
```